Status report of the baseline collimation system of the compact linear collider

J. Resta-López[1], D. Angal-Kalinin[2], B. Dalena[3], J. L. Fernández-Hernando[2], F. Jackson[2], D. Schulte[3], A. Seryi[1] and R. Tomás[3]

[1]JAI, University of Oxford, UK
[2]STFC, Daresbury, UK
[3]CERN, Geneva, Switzerland

E-mail: j.restalopez@physics.ox.ac.uk

Abstract. Important efforts have recently been dedicated to the characterisation and improvement of the design of the post-linac collimation system of the Compact Linear Collider (CLIC). This system consists of two sections: one dedicated to the collimation of off-energy particles and another one for betatron collimation. The energy collimation system is further conceived as protection system against damage by errant beams. In this respect, special attention is paid to the optimisation of the energy collimator design. The material and the physical parameters of the energy collimators are selected to withstand the impact of an entire bunch train. Concerning the betatron collimation section, different aspects of the design have been optimised: the transverse collimation depths have been recalculated in order to reduce the collimator wakefield effects while maintaining a good efficiency in cleaning the undesired beam halo; the geometric design of the spoilers has been reviewed to minimise wakefields; in addition, the optics design has been optimised to improve the collimation efficiency. This report presents the current status of the the post-linac collimation system of CLIC.

1. Introduction

The post-linac collimation systems of the future linear colliders will play an essential role in reducing the detector background at the interaction point (IP), and protecting the machine by minimising the activation and damage of sensitive accelerator components.

The CLIC Beam Delivery System (BDS), downstream of the main linac, consists of a 370 m long diagnostics section, an almost 2000 m long collimation system, and a 460 m long Final Focus System (FFS) [1, 2]. Figure 1 shows the betatron and dispersion functions along the CLIC BDS. Some relevant CLIC design parameters are shown in Table 1 for the options at 500 GeV and 3 TeV centre-of-mass (CM) energy.

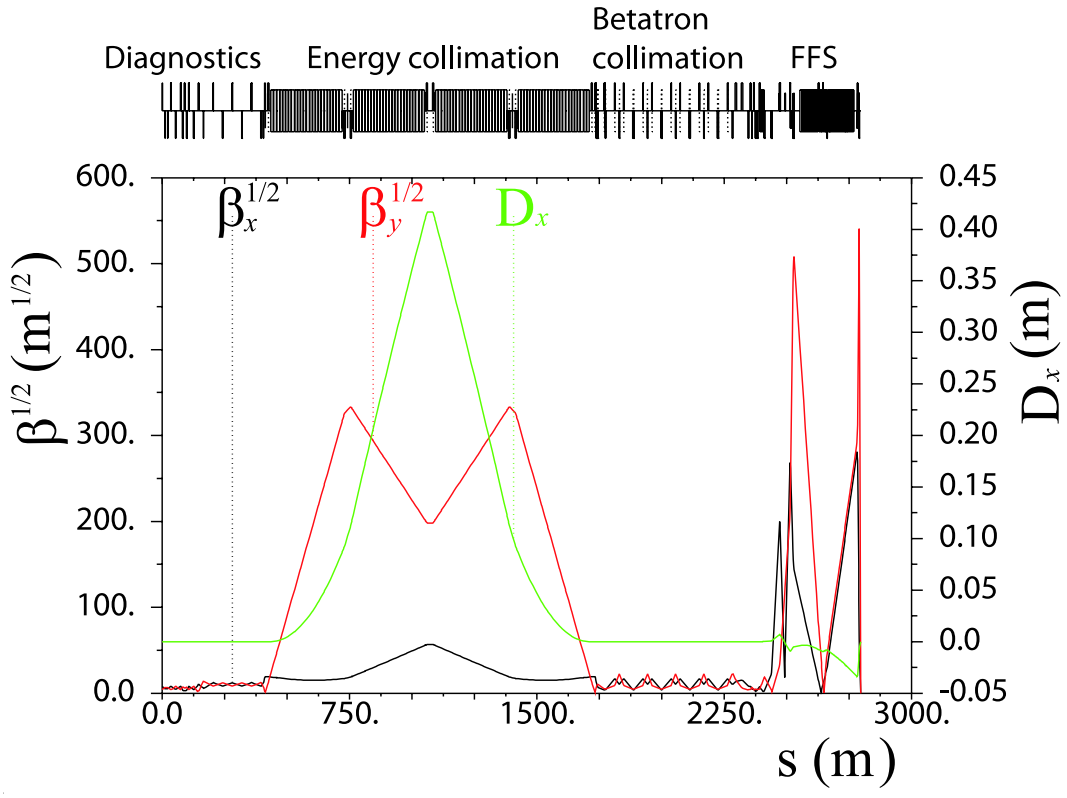

Figure 1. Optical functions of the CLIC beam delivery system.

In the CLIC BDS there are two collimation sections:

- The first post-linac collimation section is dedicated to energy collimation. The energy collimation depth is determined by failure modes in the linac [3]. A spoiler-absorber scheme (Fig. 2), located in a region with non-zero horizontal dispersion, is used for intercepting miss-steered or errant beams with energy deviation larger than 1.3% of the nominal beam energy.
- Downstream of the energy collimation section, a dispersion-free section, containing eight spoilers and eight absorbers, is dedicated to the cleaning of the transverse halo of the beam, thereby reducing the experimental background at the IP.

Table 1. CLIC parameters at 0.5 TeV and 3 TeV CM energy.

Parameter	**CLIC 0.5 TeV**	**CLIC 3 TeV**
Design luminosity (10^{34} cm^{-2}s^{-1})	2.3	5.9
Linac repetition rate (Hz)	50	50
Particles/bunch at IP ($\times 10^9$)	6.8	3.72
Bunches/pulse	354	312
Bunch length (μm)	72	44
Bunch separation (ns)	0.5	0.5
Bunch train length (ns)	177	156
Emittances $\gamma\epsilon_x/\gamma\epsilon_y$ (nm rad)	2400/25	660/20
Transverse beam sizes at IP σ_x^*/σ_y^* (nm)	202/2.3	45/0.9
BDS length (km)	1.73	2.79

The spoilers are thin devices ($\lesssim 1$ radiation length) which scrape the beam halo and, if accidentally struck by the full power beam, will increase the volume of the phase space occupied by the incident beam via multiple Coulomb scattering. In this way, the transverse density of the scattered beam is reduced for passive protection of the downstream absorber. The absorbers are usually thick blocks of material (of about 20 radiation length) designed to provide efficient halo absorption or complete removal of potentially dangerous beams.

The optics of the CLIC collimation system was originally designed by rescaling of the optics of the collimation system of the previous Next Linear Collider (NLC) project at 1 TeV centre-of-mass energy [4, 5] to the 3 TeV CLIC requirements. In the present CLIC baseline optics the length of the energy collimation section has been scaled by a factor 5 and the bending angles by a factor 1/12 with respect to the 1 TeV NLC design [6]. On the other hand, the optics of the CLIC betatron collimation section was not modified with respect to the original design of the NLC.

It is worth mentioning that, unlike the International Linear Collider (ILC) [7], where the betatron collimation section is followed by the energy collimators, in CLIC the energy collimation section is upstream of the betatron one. The main reason of choosing this lattice structure is because miss-phased or unstable off-energy drive beams are likely failure modes in CLIC, and they are expected to be much more frequent than large betatron oscillations with small emittance beams. Therefore, the energy collimation system is conceived as the first post-linac line of defence for passive protection against off-energy beams in the CLIC BDS.

Recently many aspects of the CLIC collimation system design have been reviewed and optimised towards a consistent and robust system for the Conceptual Design Report of CLIC (CLIC CDR), to be completed during 2011. In this report we describe the current status of the CLIC collimation system at 3 TeV CM energy. Here we mainly focus on the description of the collimation layout and the optimisation of the necessary

parameters of the baseline design to improve the collimation performance, only taking into account the primary beam halo. The aim is to define basic specifications of the design. Studies including secondary particle production and muon collimation are described elsewhere [8, 9].

2. Energy collimation

The beam power of the CLIC beam in the BDS with nominal parameters at 3 TeV CM energy is about 14 MW. The sustained disposal of such a high beam power during beam operation is a challenging task. Operation failures might generate errant beams which can hit and damage machine components. Therefore, machine protection, based on active and passive strategies, is required. The general CLIC Machine protection strategies are described in [10].

The CLIC energy collimation section is conceived to fulfil a function of passive protection in the BDS against miss-steered or errant beams coming from the main linac. The energy collimation depth is determined by fast failure modes which result in a significant energy deviation of the beam. For instance, possible CLIC fast ('in flight') failure modes scenarios can be caused by the effect of a missing drive beam, injection phase errors and changes in the charge of the main beam [3].

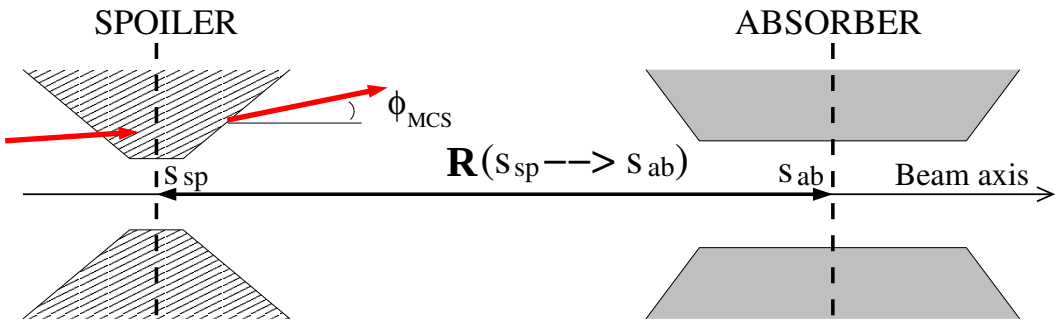

Figure 2. Basic spoiler-absorber scheme.

The CLIC energy collimation system consists of a spoiler-absorber scheme (see Fig. 2), located in a region with non-zero horizontal dispersion. The lattice layout of the CLIC energy collimation section is shown in Fig. 3. The corresponding optical parameters and transverse beam size at the energy spoiler and absorber are indicated in Table 2.

The selection of the material to make the spoiler is basically determined by the electrical, thermal and mechanical properties of the material. Regarding the survival condition of the energy spoiler, the robustness of the material is crucial. At the same time, a spoiler with high electrical conductivity is desired to avoid intolerable wakefield effects. Earlier studies of the CLIC spoiler heating and spoiler damage limit [11] concluded that a spoiler made of beryllium (Be) might be a suitable solution in terms of high robustness and acceptable wakefields. On the other hand, in the current design

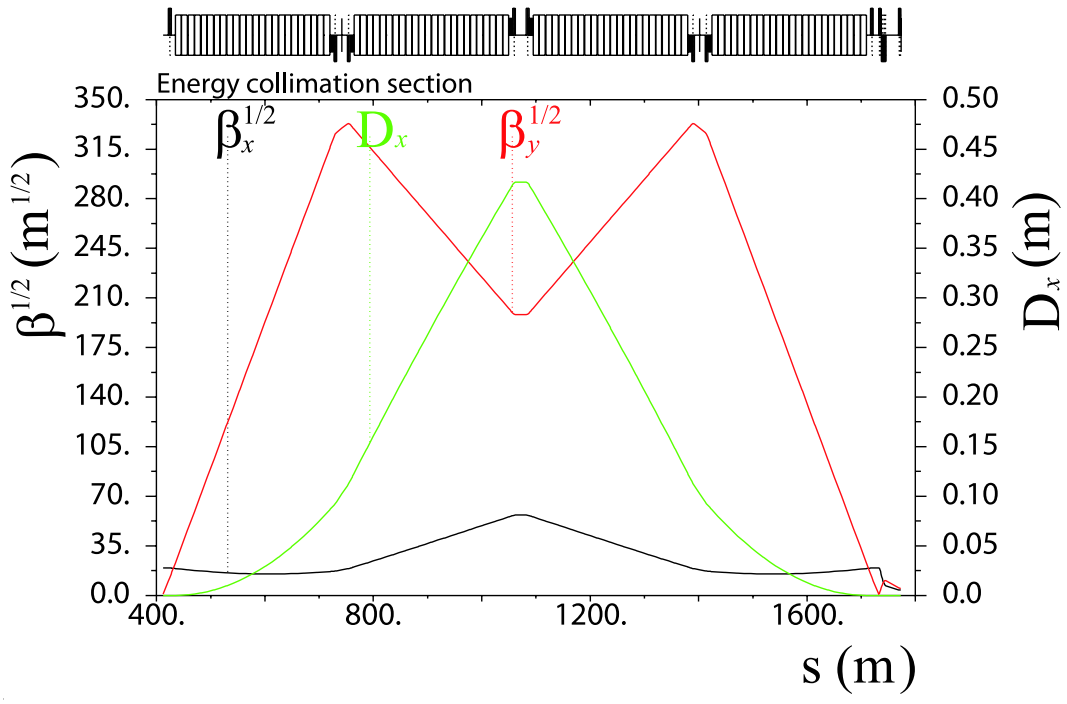

Figure 3. Optical functions of the CLIC energy collimation section: horizontal dispersion and square root of the betatron functions.

Table 2. Optics and beam parameters at collimator position for energy collimation: longitudinal position (s), horizontal and vertical β-functions (β_x and β_y), horizontal dispersion (D_x), horizontal and vertical rms beam sizes (σ_x and σ_y). In this case a uniform energy distribution with 1% full width energy spread has been considered.

Name	s [m]	β_x [m]	β_y [m]	D_x [m]	σ_x [μm]	σ_y [μm]
ENGYSP (spoiler)	907.098	1406.33	70681.87	0.27	779.626	21.945
ENGYAB (absorber)	1072.098	3213.03	39271.54	0.416	1201.189	16.358

the CLIC absorbers are made of titanium alloy (90% Ti, 6% Al, 4% V) with copper (Cu) coating.

The collimation depth of the spoiler has been set to intercept beams with energy deviation larger than 1.3% of the nominal beam energy. The horizontal aperture for the energy collimator is then set to $a_x = D_x\delta_{\text{aper}}$, with D_x the horizontal dispersion at the spoiler position and $\delta_{\text{aper}} = \pm 1.3\%$.

It is necessary to point out that the energy collimation system, with a total length of 1400 m, is the longest part of the BDS. This space is filled almost entirely with bending magnets to generate the required horizontal dispersion. The length of the energy collimation system is determined by a trade-off between the following requirements:

- The beam spot size at the collimators must be sufficiently large for passive protection. The energy collimators are required to withstand the impact of a full

bunch train of nominal emittance.

- The emittance growth due to synchrotron radiation emission must be constrained within tolerable levels.
- the half gap a_x must be big enough to minimise the near-axis wakefield effects on the beam during normal operation of the machine.

For a given lattice the horizontal emittance growth due to incoherent synchrotron radiation can be evaluated using the following expression [12]:

$$\Delta(\gamma\epsilon_x) \simeq (4.13 \times 10^{-8}\ \mathrm{m^2GeV^{-6}})E^6 I_5\ , \tag{1}$$

as a function of the beam energy E and the so-called radiation integral I_5, which is defined as [13],

$$I_5 = \int_0^L \frac{\mathcal{H}}{|\rho_x^3|}\, ds = \sum_i L_i \frac{\langle\mathcal{H}\rangle_i}{|\rho_{x,i}^3|}\ , \tag{2}$$

where the sum runs over all bending magnets, with bending radius ρ_i, length L_i, and the average of the function $\mathcal{H}$, which is defined by:

$$\mathcal{H} = \frac{D_x^2 + (D_x'\beta_x + D_x\alpha_x)^2}{\beta_x}\ , \tag{3}$$

where β_x and $\alpha_x = -(1/2)d\beta_x/ds$ denote the typical twiss parameters, D_x the dispersion function and $D_x' = dD_x/ds$.

For the CLIC collimation system $I_5 \simeq 1.9 \times 10^{-19}$ m^{-1}, and then $\Delta(\gamma\epsilon_x) \simeq 0.089$ μm. This means about 13.5% emittance growth respect to the design emittance $\gamma\epsilon_x = 0.66$ μm. This corresponds to a beam core luminosity loss of $\Delta\mathcal{L}/\mathcal{L}_0 = 1 - 1/\sqrt{1+\Delta(\gamma\epsilon_x)/(\gamma\epsilon_x)} \simeq 6\%$. For the total CLIC BDS (including the CLIC collimation system and the FFS) it results $I_5 \simeq 3.8 \times 10^{-19}$ m^{-1} and an emittance growth of $\Delta(\gamma\epsilon_x)/(\gamma\epsilon_x) \simeq 27.3\%$. This translates into a total luminosity loss of about 11.4%. This value is much lower than the result of 24% obtained in Ref. [14] from beam tracking simulations. This discrepancy is basically due to the fact that our calculation from Eqs. (1) only considers the effect from the radiation emission due to the deflection of the beam by the bending magnets, while the tracking simulations also take into account the additional effect from the optical nonlinearities of the lattice.

In the following sections we describe the design of the spoiler and absorber based on survival considerations and, by means of simulations, the thermo-mechanical performance of the spoiler is investigated in detail for the worst damage scenario from a full bunch train impact. Collimation efficiency simulation studies are also performed in order to optimise the collimation apertures.

2.1. Spoiler and absorber design

This section is devoted to the optimisation of the geometric dimensions of the energy spoiler and absorber, considering the geometry of Fig. 4. The design parameters of the energy spoiler and absorber are shown in Table 3.

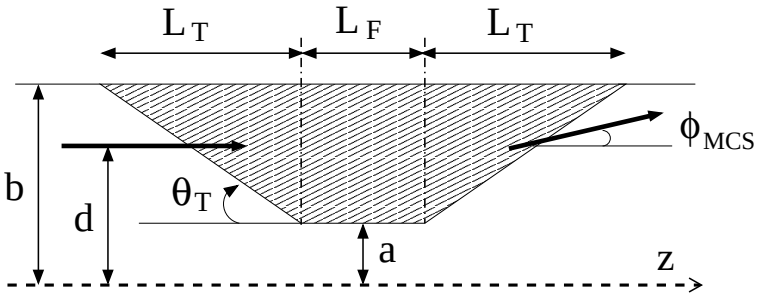

Figure 4. Spoiler and absorber jaw longitudinal view.

Table 3. Design parameters of the CLIC energy spoiler and absorber.

Parameter	ENGYSP (spoiler)	ENGYAB (absorber)
Geometry	Rectangular	Rectangular
Hor. half-gap a_x [mm]	3.51	5.41
Vert. half-gap a_y [mm]	8.0	8.0
Tapered part radius b [mm]	8.0	8.0
Tapered part length L_T [mm]	90.0	27.0
Taper angle θ_T [mrad]	50.0	100.0
Flat part length L_F [radiation length]	0.05	18.0
Material	Be	Ti alloy–Cu coating

2.1.1. Absorber protection. The main function of the spoiler is to provide sufficient beam angular divergence by multiple Coulomb scattering (MCS) to decrease the transverse density of an incident beam, thereby reducing the damage probability of the downstream absorber and any other downstream component. This condition determines the minimum length of the material traversed by the beam in the spoiler, i.e. the flat part of the spoiler body ($L_F \neq 0$).

Beam particles traversing the spoiler material are deflected by MCS. The transverse root mean square (rms) scattering angle experienced by the beam particle at the exit of the spoiler can be calculated using the well known Gaussian approximation of the Molière formula [15]:

$$\phi_{MCS} = \frac{13.6\ [\mathrm{MeV}]}{\beta cp} z \sqrt{\frac{\ell}{X_0}} \left[1 + 0.038 \ln\left(\frac{\ell}{X_0}\right)\right] , \tag{4}$$

where X_0 is the radiation length of the spoiler material, ℓ is the length of material traversed by the beam particle, β is the relativistic factor ($\beta \simeq 1$ for ultra-relativistic beams), c the speed of light, p the beam momentum, and z is the charge of the incident particle ($z = 1$ for electrons and positrons). Equation (4) is accurate to 11% or better for $10^{-3} < \ell/X_0 < 100$. The square of the transverse angular divergence of a beam at the exit of the spoiler is given by $\langle x'^2_{sp}\rangle = \langle x'^2_{sp0}\rangle + \phi^2_{MCS}$, and $\langle y'^2_{sp}\rangle = \langle y'^2_{sp0}\rangle + \phi^2_{MCS}$ for the

horizontal and vertical plane, respectively. The terms $\langle x'^2_{sp0}\rangle$ and $\langle y'^2_{sp0}\rangle$ refer to the initial angular components at the entrance of the spoiler and are usually much smaller than the scattering angular component. Taking into account the linear transport, the expected value of the square of the horizontal and vertical displacements at the downstream absorber can be approximated by

$$\langle x^2_{ab}\rangle \simeq R^2_{12}(s_{sp}\rightarrow s_{ab})\phi^2_{MCS} + D^2_x\sigma^2_\delta \ , \tag{5}$$

$$\langle y^2_{ab}\rangle \simeq R^2_{34}(s_{sp}\rightarrow s_{ab})\phi^2_{MCS} \ . \tag{6}$$

In Eq. (5) the dispersive component $D^2_x\sigma^2_\delta$ has been taken into account, with $D_x = 0.416$ m the horizontal dispersion at the energy absorber position, and $\sigma_\delta = \sqrt{\langle\delta^2_E\rangle - \langle\delta_E\rangle^2}$ the rms beam energy spread. $\delta_E \equiv \Delta E/E_0$ represents the energy deviation, with E_0 the nominal beam energy. $R_{12}(s_{sp}\rightarrow s_{ab}) = 160.75$ m and $R_{34}(s_{sp}\rightarrow s_{ab}) = 169.26$ m are the corresponding linear transfer matrix elements between the energy spoiler and absorber. For beam energy 1500 GeV and length of the spoiler material $\ell < 1\ X_0$ the rms angular divergence by MCS is $\phi_{MCS}\sim 1\ \mu$rad. If one considers energy spread values $\sigma_\delta \approx 0.29\%$, the energy dispersive term $D_x\sigma_\delta$ is dominant in Eq. (5), and we can approximate the transverse beam size at the absorber position s_{ab} by:

$$\sigma_x(s_{ab}) = \sqrt{\langle x^2_{ab}\rangle} \simeq D_x\sigma_\delta \ , \tag{7}$$

$$\sigma_y(s_{ab}) = \sqrt{\langle y^2_{ab}\rangle} \simeq R_{34}(s_{sp}\rightarrow s_{ab})\phi_{MCS} \ . \tag{8}$$

For the protection of an absorber made of Ti alloy, the following limit for the radial beam size can be established [4, 16]:

$$\sigma_r(s_{ab}) = \sqrt{\sigma_x(s_{ab})\sigma_y(s_{ab})} \gtrsim 600\ \mu\text{m} \ . \tag{9}$$

Using Eqs. (7) and (8), the constraint (9) can be rewritten as follows:

$$\sqrt{|R_{34}(s_{sp}\rightarrow s_{ab})|D_x\sigma_\delta\phi_{MCS}} \gtrsim 600\ \mu\text{m} \ . \tag{10}$$

In terms of the transverse particle density peak, the condition for absorber survival can be written as:

$$\hat{\rho}(s_{ab}) = \frac{N_e}{2\pi\sigma^2_r(s_{ab})} \lesssim 1.64\times 10^9 \text{ particles/mm}^2 \text{ per bunch} \ , \tag{11}$$

where $N_e = 3.72\times 10^9$ is the number of particles per bunch.

Considering a Gaussian beam energy distribution with $\sigma_\delta = 0.5\%$ energy spread width, from the constraint (10) one obtains that $\phi_{MCS} \gtrsim 10^{-6}$ rad ensures the absorber survival. From this condition and using Eq. (4) one can determine the minimum length of spoiler material necessary to guarantee the absorber survival. This condition is fulfilled if the Be spoiler (Fig. 4) is designed with a central flat part of length $L_F \gtrsim 0.02\ X_0$.

Similar results are obtained considering a beam with a uniform energy distribution of $A_\delta = 1\%$ full energy spread and where $\sigma_\delta = A_\delta/\sqrt{12}$.

In order to validate these results tracking simulations of bunches have been performed through the CLIC BDS, with 50000 macroparticles per bunch, using the code PLACET [17]. In this beam model a macroparticle represents a large number of electrons (or positrons) with nearly the same energy and phase space position. For instance, macroparticle i is represented by a 6-D phase space vector $(x_i, x'_i, y_i, y'_i, z_i, E_i)$, by a number of second moments‡, and by a weight proportional to the number of particles it represents.

Assuming all particles of the beam hit the energy spoiler and full beam transmission through the spoiler, and applying MCS, we have calculated the transverse beam spot size $\sigma_r = \sqrt{\sigma_x \sigma_y}$ and its corresponding transverse beam density at the energy absorber. From the tracking simulations of the 50000 macroparticles of one bunch, σ_x and σ_y are calculated from the rms of the x and y positions of the macroparticle distribution. Figure 5 compares the result of σ_r at the absorber position as a function of the spoiler length (in units of radiation length) traversed by the beam for the following cases: a monochromatic beam, i.e. with no energy spread, and a beam with a uniform energy distribution of 1% full spread. The results from the tracking simulations are compared with those from analytical calculations using Eqs. (7) and (8). The corresponding results in terms of transverse particle density are shown in Fig. 6. For a realistic case of a beam with 1% of energy spread, selecting a length for the energy spoiler of about 0.05 X_0 might be enough to ensure the survivability of the downstream absorber in case of a full impact of the beam.

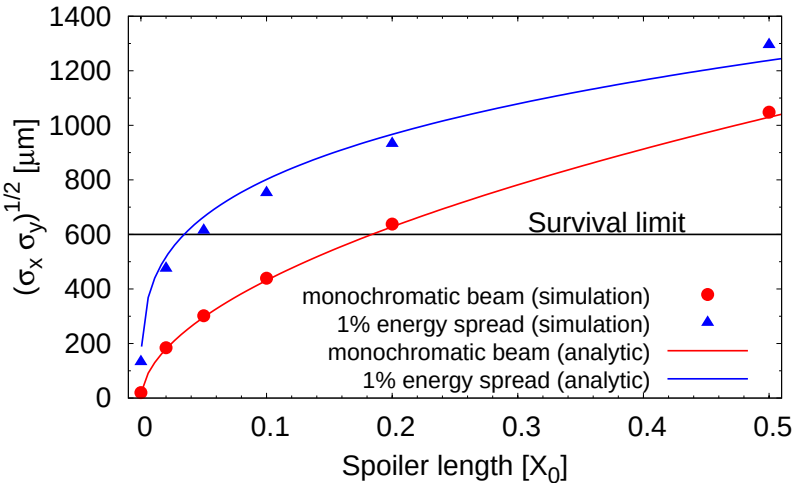

Figure 5. Transverse spot size at the energy absorber position as a function of the upstream spoiler length.

‡ The second moments are the covariances of transverse phase coordinates for all particles represented by the macroparticle.

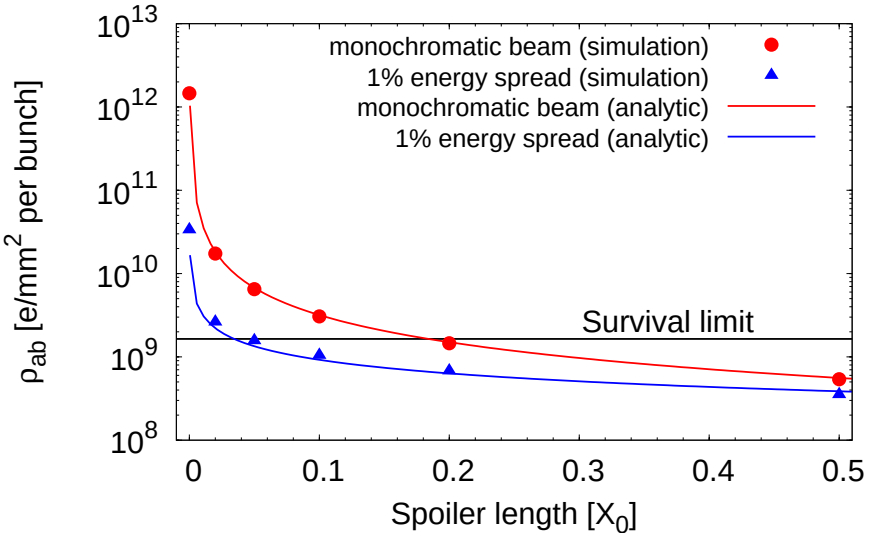

Figure 6. Transverse beam density at the energy absorber position as a function of the upstream spoiler length.

2.1.2. Spoiler protection. Based on the SLC experience§, energy errors in the linac are expected to occur much more frequently than orbit disruptions of on-energy beams. Therefore, the E-spoiler has to be designed robust enough so that it survives without damage from the impact of an entire bunch train in case of likely events generating energy errors.

The instantaneous heat deposition is the principal mechanism leading to spoiler/collimator damage. The main sources of such a heating are the energy deposition by direct beam-spoiler material interaction, the image current heat deposition and the electric field breakdown. The most critical case is the instantaneous temperature rise in the spoiler due to a deep beam impact. Since the thickness of the spoiler is significantly small in terms of radiation length ($L_F \ll 1\ X_0$), electrons/positrons deposit energy basically by ionization, and practically no electromagnetic showers are developed.

As an approximate criterion for spoiler survival the following condition can be established: the instantaneous temperature increment due to the impact of a full bunch train on the spoiler ($\Delta\hat{T}_{\rm inst}$) must be lower than the temperature excursion limit for melting ($\Delta T_{\rm melt}$) and the temperature excursion limit for fracture of the material by thermal stress ($\Delta T_{\rm fr}$), i.e.

$$\Delta\hat{T}_{\rm inst} = \frac{1}{\varrho C_p}\left(\frac{dE}{dz}\right)\frac{N_e N_b}{2\pi\sigma_x\sigma_y} < \min[\Delta T_{\rm fr}, \Delta T_{\rm melt}]\ , \tag{12}$$

where ϱ is the density of the spoiler material, C_p is the heat capacity, N_e the bunch population and N_b the number of bunches per train. The safe limit is below the minimum between the thermal stress temperature limit $\Delta T_{\rm fr}$ and the melting limit $\Delta T_{\rm melt}$. Generally the minimum corresponds to $\Delta T_{\rm fr}$.

§ The Stanford Linear Collider (SLC) [27] is the sole linear collider built to date.

Here the energy deposition per unit length is denoted as (dE/dz), whose value can be determined using the formula for the collision stopping power given in Ref. [18] in the high energy limit:

$$\frac{1}{\varrho}\left(\frac{dE}{dz}\right) = 0.153536\frac{Z}{A}B(T)\ , \tag{13}$$

where Z/A is the ratio of the number of electrons in the atom to the atomic weight of the spoiler material, and $B(T)$ is the stopping number defined in [18]. It is necessary to mention that Eq. (13) gives a conservative estimation of the energy deposited in the spoiler and overestimates it, since by definition the stopping power is the energy lost by the passing beam, and not the energy that is actually deposited in the target. A fraction of the lost energy might indeed escape from the spoiler.

Table 4 shows the instantaneous increment of temperature calculated using Eqs. (12) and (13) for CLIC electron and positron beams and for different spoiler materials. For these calculations we have neglected the temperature dependence of the heat capacity C_p and used the following rms transverse beam sizes: $\sigma_x = 779.6$ μm and $\sigma_y = 21.9$ μm. The material properties of Table 5 have been considered. These material data have been obtained from Ref. [19].

Table 4. Energy deposition per unit length (dE/dz) estimated from Eq. (13) for a CLIC beam traversing a thin spoiler, and instantaneous temperature increment calculated using Eq. (12). Different spoiler materials are compared.

Spoiler	**Electron beam**		**Positron beam**	
Material	dE/dz [MeV/cm]	$\Delta\hat{T}_{inst}$ [K]	dE/dz [MeV/cm]	$\Delta\hat{T}_{inst}$ [K]
Be	4.4003	214	4.3181	209
C	6.001	648	5.8879	636
Ti	10.8487	786	10.6406	770
Cu	20.9522	1049	20.5422	1028
W	39.1714	2606	38.3897	2554

Table 5. Material properties: atomic number Z, mass number A, material density ϱ, specific heat capacity C_p, electrical conductivity σ (at room temperature, 293 K) and radiation length X_0.

Material	Z	A [g/mol]	ϱ [gm^{-3}]	C_p [Jg^{-1}K^{-1}]	σ [Ω^{-1}m^{-1}]	X_0 [m]
Be	4	9.01218	1.84×10^6	1.925	2.3×10^7	0.353
C	6	12.0107	2.25×10^6	0.708	1.7×10^4	0.188
Ti	22	47.867	4.5×10^6	0.528	1.8×10^6	0.036
Cu	29	63.546	8.93×10^6	0.385	5.9×10^7	0.014
W	74	183.84	19.3×10^6	0.134	1.8×10^7	0.0035

The rapid heating of the material caused by the impact of the train in the spoiler may contribute to the fracture of the material by thermal stress. The increment of temperature which determines the limit for thermal fracture can be analytically evaluated using the following expression:

$$\Delta T_{\rm fr} \cong \frac{2\sigma_{\rm UTS}}{\alpha_T Y} \ , \tag{14}$$

where $\sigma_{\rm UTS}$ is the ultimate tensile strength, α_T is the thermal expansion coefficient and Y is the modulus of elasticity (or Young modulus). The ultimate tensile strength is defined as the maximum stress that the material can withstand. It is necessary to mention that for the value of $\sigma_{\rm UTS}$ discrepancies of up to 40% can be found between different bibliographic sources about material data. Here we have used the material information from Ref. [19], which gives a pesimitic value for $\sigma_{\rm UTS}$ in comparison with other bibliographic sources.

For the CLIC energy spoiler made of Be, using the mechanical and thermal properties of Table 6, we obtain $\Delta T_{\rm fr} \simeq 228$ K, which is slightly bigger than the values obtained for $\Delta\hat{T}_{inst}$ for a Be spoiler (see Table 4). Therefore, according this analytic calculation the Be spoiler is below, but close, the fracture limit in case of the impact of an entire CLIC bunch train.

Table 6. Summary of material properties for beryllium.

Young modulus, Y [10^5 MPa]	2.87
Thermal expansion coefficient, α_T [10^{-6} K^{-1}]	11.3
Ultimate tensile strength, $\sigma_{\rm UTS}$ [MPa]	370
Tensile yield strength [MPa]	240
Compressive yield strength [MPa]	270
Specific heat capacity, C_p [J/(gK)]	1.925
Density, ϱ [g/cm^3]	1.84

In general Eq. (14) may be a good approximation to estimate the temperature at which the material may crack. However, it is necessary to point out that Eq. (14) is commonly used with quasi-static material data and for fatigue purposes. In the case of the spoiler heating by the beam we are not involved in a fatigue process but in a "one-time" accident scenario. It is known that when a beam hits a material the energy is deposited very quickly into it. This causes a rapid expansion of the material, and hence quasi-static material properties will not give an accurate answer. In this case, the materials under study need to be characterised dynamically in order to give more valid results. For a more precise thermo-mechanical characterisation of the spoiler material numerical simulations are usually performed using tools such as FLUKA [20] and ANSYS [21]. Simulation results are shown in the next section.

2.1.3. Thermo-mechanical analysis of the spoiler. In order to evaluate the robustness of the spoiler, simulations, using the codes FLUKA and ANSYS, have been made considering the geometrical parameters of the CLIC E-spoiler made of Be, and assuming the nominal parameters of the CLIC beam.

The following horizontal and vertical beam sizes at the spoiler position have been assumed‖: $\sigma_x = 779$ μm and $\sigma_y = 21.9$ μm. The bunch train impact was simulated using FLUKA. Figure 7 shows the energy deposition in the spoiler as the beam traverses it. A transverse position depth of $d \simeq 7.8$ mm (see Fig. 4) for the beam was chosen, to maximise the total amount of material that it would face in case of a pessimistic accident scenario. This represents a deviation of about 10 σ_x from nominal orbit. Figure 8 shows the corresponding peaks of energy density along the beam track in the spoiler material. The peak of energy deposition happens in the edge of the trailing taper and is about 5.4 GeV/cm^3 per incident particle; using the specific heat and density values of beryllium, shown in Table 6, and the total number of particles in a CLIC bunch train, $N_b \times N_e = 1.16 \times 10^{12}$, a temperature increment of approximately 570 K is obtained.

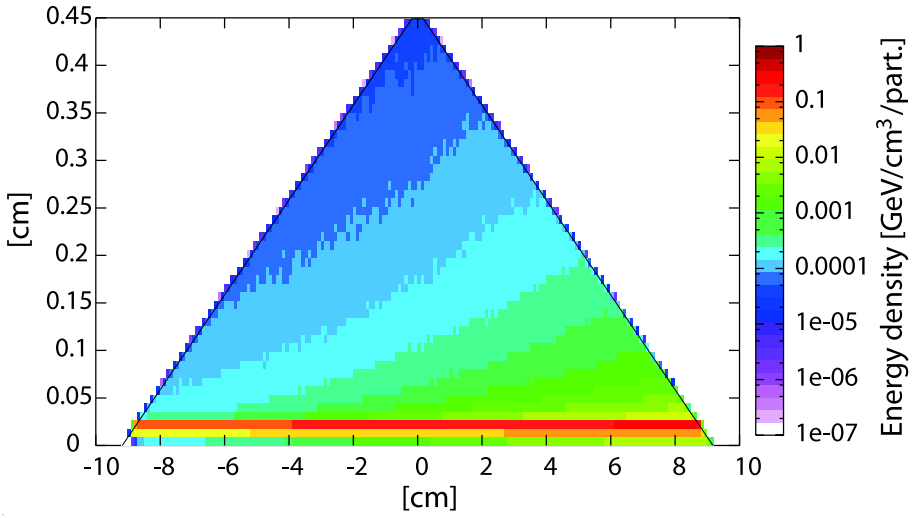

Figure 7. Energy density deposition normalised per incident particle for a CLIC beam hitting the spoiler.

In order to perform the transient analysis of the CLIC train hitting the Be E-spoiler, the FLUKA result was transformed into an ANSYS input and applied in a spoiler model. The results are recorded after the beam has hit the spoiler to determine if there would be any stress build up that could reach fracture levels. The results of the stress calculations in the Be can be compared with the mechanical stress limits of the material by means of a certain failure criterion expressed by the equivalent stress

‖ $\sigma_x = 779$ μm at spoiler position corresponds to the rms horizontal beam size of a beam with a uniform energy spread of 1% full width. However, in this FLUKA simulation we have assumed the nominal energy for all particles of the beam and no energy spread. This assumption gives more pessimistic predictions than a more realistic situation.

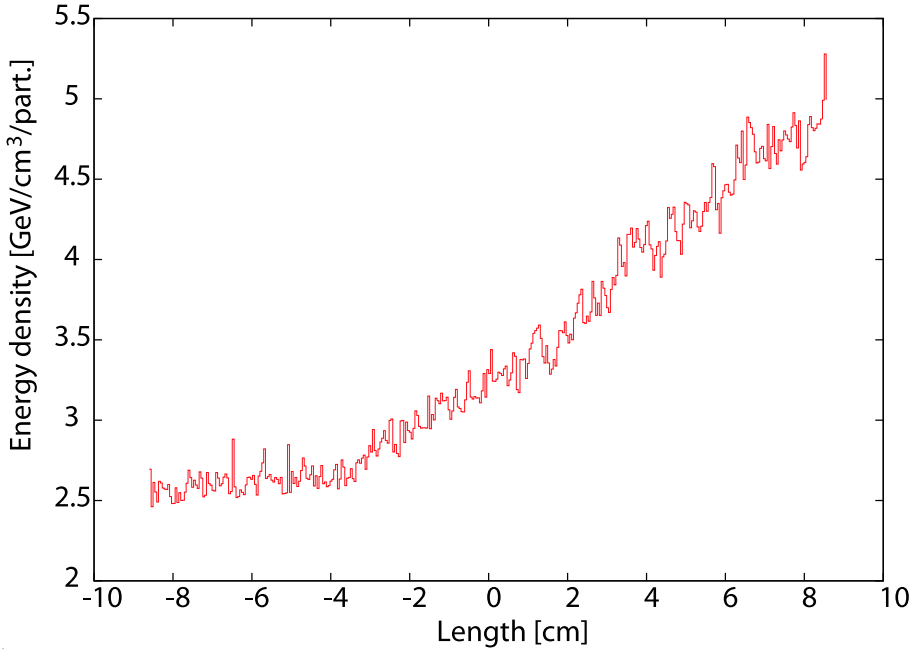

Figure 8. Peaks of energy density deposition normalised per incident particle for a CLIC beam hitting the spoiler.

values¶:

$$\sigma_{eq} = \frac{1}{\sqrt{2}}\sqrt{(\sigma_1 - \sigma_2)^2 + (\sigma_2 - \sigma_3)^2 + (\sigma_3 - \sigma_1)^2}\ , \tag{15}$$

where σ_1, σ_2 and σ_3 are the principal stresses at a given position in the three main directions of the working coordinate system, which in our case is Cartesian. Figure 9 shows the equivalent stress calculated using ANSYS on the spoiler body 3 μs after the full CLIC bunch train has hit it, time at which the stress reaches its maximum and stabilises, with an impact depth of $d \simeq 7.8$ mm. In this case we obtain a top equivalent stress of ≈ 950 MPa, and tensile, which is way above the ultimate tensile strength limit, thus reaching fracture levels.

Let us now consider another case of impact in which the beam traverses less quantity of material. For instance, the case of the beam hitting the spoiler with impact depth $d = 3.7$ mm, which means a deviation of about 5 σ_x with respect to the nominal beam axis. Figure 10 shows the equivalent stress calculated using ANSYS, after 11 μs, the time needed in this case for the stress to reach its peak and stabilise over that top value. The maximum value of stress after a CLIC bunch train has hit the spoiler is about 240 MPa, and compressive, value that corresponds to the yield compressive strength value. In this situation there will not be fracture, but there might be a permanent deformation. This

¶ This equivalent stress is also called *von Mises stress* [22], and is often used for metals under multi-axial state stress. It allows any arbitrary three-dimensional stress state to be represented as a single positive stress value. Equivalent stress is part of the maximum equivalent stress failure theory used to predict the onset of yielding and to describe the post-yielding response.

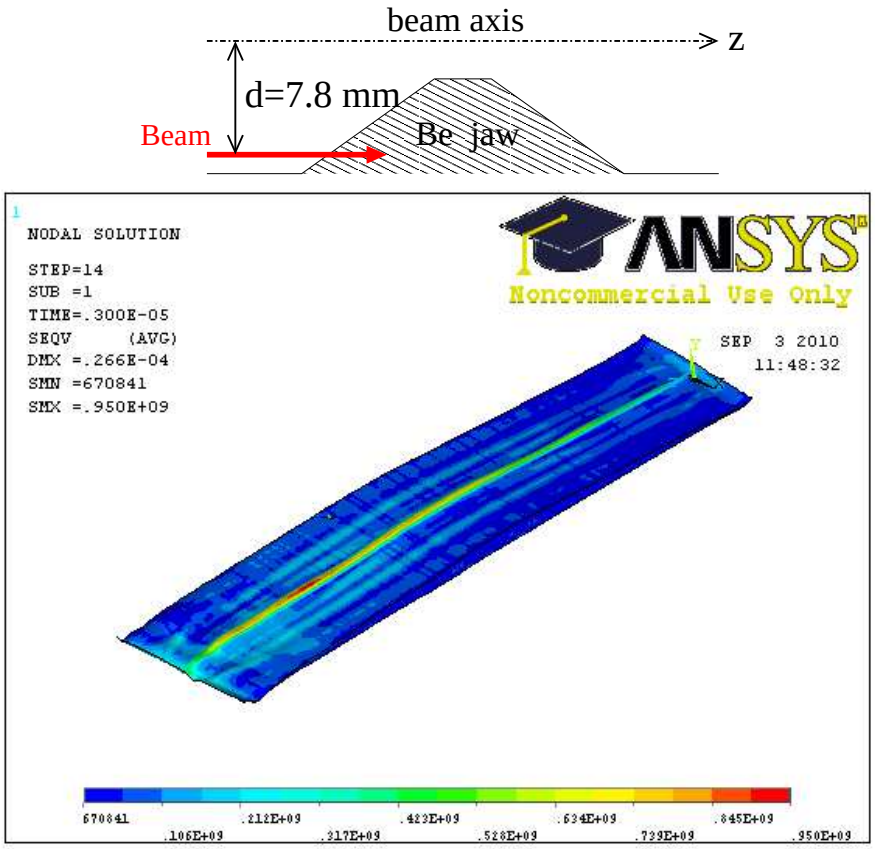

Figure 9. Equivalent stress on the spoiler body 3 microseconds after a CLIC bunch train hits it. In this case the transverse impact depth is $d = 7.8$ mm, which corresponds to a beam deviation of 10 σ_x with respect to the beam axis.

deformation translates into horizontal protuberances of ~ 1 μm, which represents 0.03% of the minimum half gap of the E-spoiler. This might have consequences in terms of degradation of the beam stability and emittance blow-up by increasing the collimator wakefield effects. The additional wakefield effects due to the deformation of the spoiler are evaluated in Section 4.3.

Above we have considered two cases of impact position on the spoiler surface: a big transverse impact depth of about 10 σ_x from the nominal beam axis, and a more optimistic scenario with an impact depth of about 5 σ_x. These two examples, one more pessimistic than the other, have allowed us to obtain a preliminary estimate of the survivability of the CLIC E-spoiler. However, the impact position of the beam on the spoiler surface depends on failure scenarios, and a detailed study of these failure events affecting the beam energy would be useful in order to determine the most likely angles and positions of impact for a more precise risk analysis.

Another necessary remark is that this study has been performed for a perfect beryllium structure, i.e. without any imperfections or impurities, which could act as a stress concentrator. Therefore, Be samples will need to be tested to compressive stress

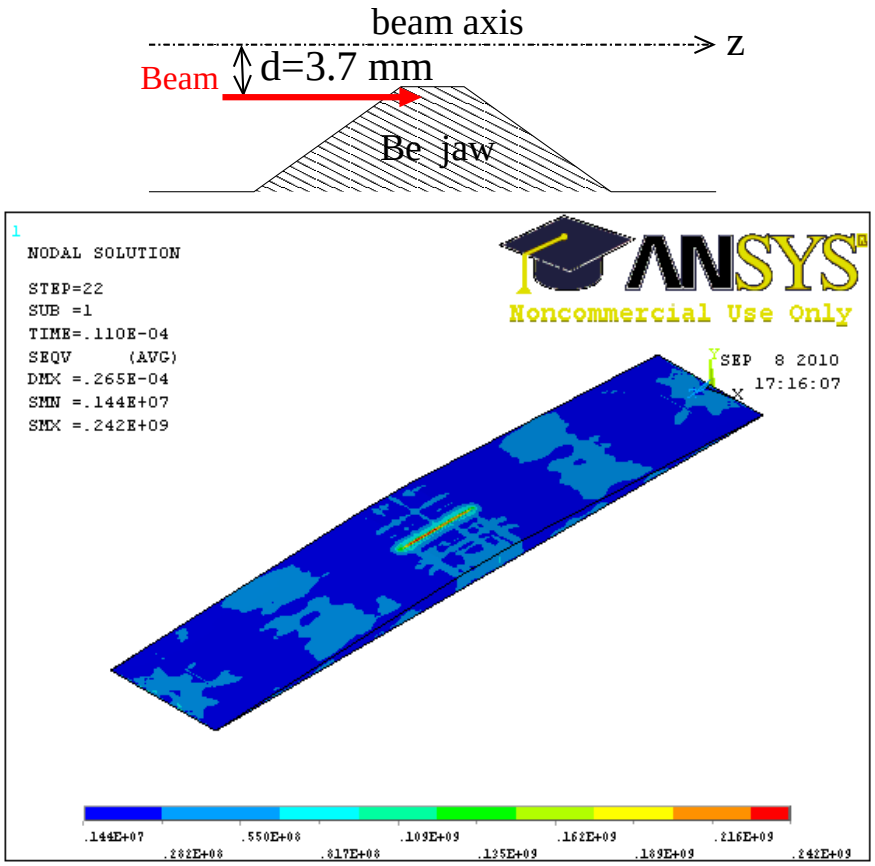

Figure 10. Equivalent stress on the spoiler body 11 microseconds after a CLIC bunch train hits it. In this case, the transverse impact depth is $d = 3.7$ mm, which corresponds to a beam deviation of 4.8 σ_x with respect to the beam axis.

up to 200 MPa to assess their suitability for spoiler manufacturing.

2.2. Collimation efficiency

In this section the capability of the system to intercept off-energy beams is investigated by means of particle tracking simulations.

Let us assume complete transmission of the beam through the E-spoiler[+] and perfect collimation at the absorber, i.e. particles hitting the absorber are considered totally lost without production of secondary particles. With these assumptions, a beam of initial energy offset 1.5% of the nominal energy and 1% full energy spread has been tracked through the CLIC BDS using the code PLACET. Figure 11 shows the horizontal and vertical phase space at the exit of the E-spoiler, taking into account the effect of MCS for different cases of traversed spoiler length in units of radiation length (X_0). The tracking results show how the transverse beam phase space area increases at the spoiler

[+] This approximation is only valid for very thin spoilers (less than 1 radiation length) made of materials with low Z.

exit as the spoiler length increases. In Fig. 11 (Left) the results also show that part of the beam (with x amplitude < 3.5 mm) does not hit the spoiler and is not scattered by MCS. To avoid this, if we demand a complete interception of the off-energy beam (with the above energy conditions), the E-spoiler half gap has to be reduced further, to about 2.5 mm. Reducing the spoiler half gap, the wakefield effects increase. This may be a possible cause for concern. However, as we will see in Section 4, the contribution of the E-spoiler to the wakefields is practically negligible due to its relative large half gap (3.5 mm) in comparison with that of the betatron spoilers ($\sim$ 100 μm), which significantly contribute to the collimator wakefields for small position offsets from the orbit axis. Reducing the E-spoiler half gap to 2.5 mm might still give a tolerable stability margin in terms of wakefields.

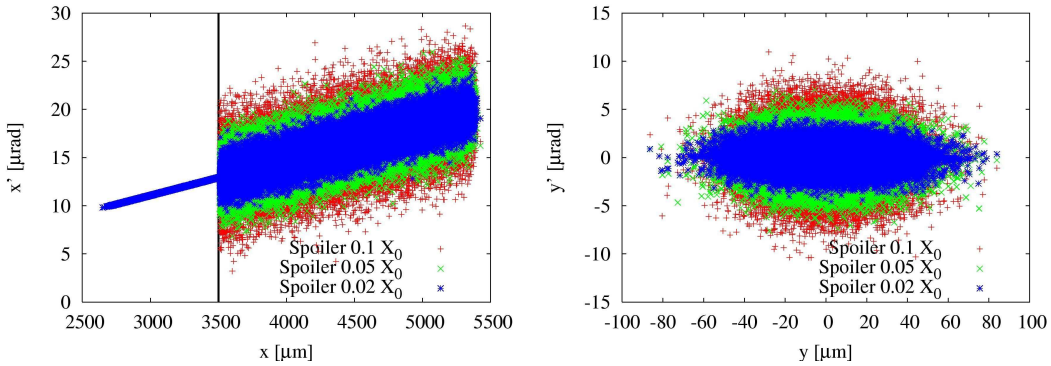

Figure 11. Left: x–x' phase space at the exit of the spoiler. Right: y–y' phase space at the exit of the spoiler. The following cases of traversed spoiler length are represented: 0.02 X_0, 0.05 X_0 and 0.1 X_0. The collimation limit, determined by the edge of the spoiler jaw, is represented by the vertical black line.

Figure 12 shows the horizontal and vertical distribution of the beam particles at the E-absorber. Particles with amplitude $x > 5.41$ mm are perfectly absorbed. However, part of the beam does not hit the absorber jaw and is propagated downstream, with risk of hitting some sensible components of the lattice or at the interaction region. Where are these particles deposited? In order to study the efficiency of the energy collimation system to intercept a miss-steered beam with centroid energy offset $\gtrsim 1.5\%$, the particle loss map along the CLIC BDS has been studied via tracking simulations. As expected, the main particle losses are concentrated at the absorber (see Fig. 13). However, with the current absorber aperture, $a_x = 5.41$ mm, only 70% of the miss-steered beam is collimated. Considering a beam pipe radius of 8 mm in the BDS, approximately 10% of beam losses occur in a region just upstream of the E-absorber. These residual losses of primary beam particles in non-dedicated collimation places (uncontrolled losses) hit the beam-pipe or other parts of lattice elements, thus creating additional fluxes of muons and other secondary particles which propagate downstream. To avoid uncontrolled particle losses, a possible solution could be the increase of the beam pipe radius from the current

design 8 mm to a new value of about 10 mm *.

If the absorber aperture is reduced to $a_x = 4.0$ mm, practically 100% of the beam is stopped at the E-absorber.

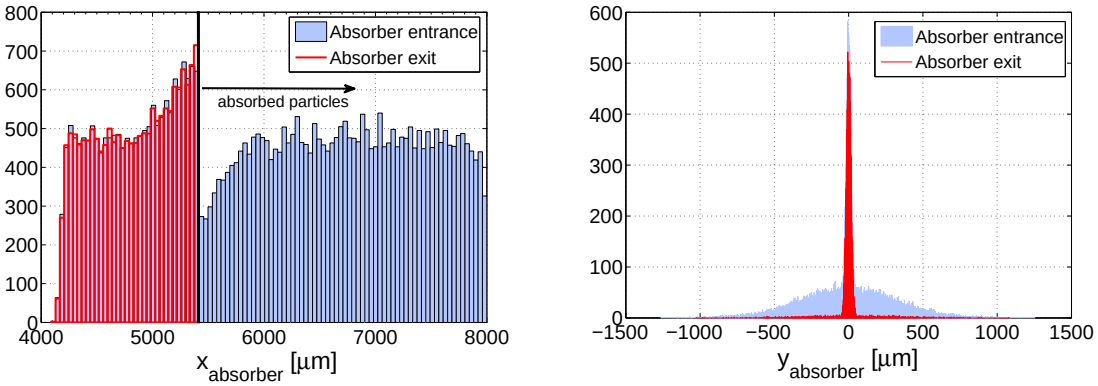

Figure 12. Transverse beam distribution at the E-absorber entrance and exit, considering a beam with 1.5% centroid energy offset and a uniform energy distribution with 1% full width of energy spread. Projection on the horizontal plane (Left), and projection on the vertical plane (Right). The collimation limit determined by the edge of the absorber jaw is represented by the vertical black line.

3. Betatron collimation

The main function of the betatron collimation section is the removal of any particle from the transverse halo of the primary beam, i.e. beam particles with large betatron amplitudes, which can cause unacceptable experimental background levels in the interaction region. In addition, the collimation system design must limit the regeneration of halo due to optical or collimator wakefield effects. The optics of the betatron collimation section is shown in Fig. 14. The values of the betatron functions and transverse beam size at each betatron collimator (spoiler and absorber) position are indicated in Table 7.

In order to provide an acceptable cleaning efficiency of the transverse beam halo the betatron collimation depths are determined from the following conditions:

- Minimisation of the synchrotron radiation photons in the first final quadrupole magnet (QF1) that can hit the second final quadrupole (QD0).
- Minimisation of the beam particles that can hit either QF1 or QD0.
- Neither synchrotron radiation photons nor electrons (positrons) of the beam are permitted to impact the detector or its mask.

* Parallel and complementary studies, based on resistive wall effect in the CLIC BDS, have also suggested an optimum beam pipe radius of 10 mm [23].

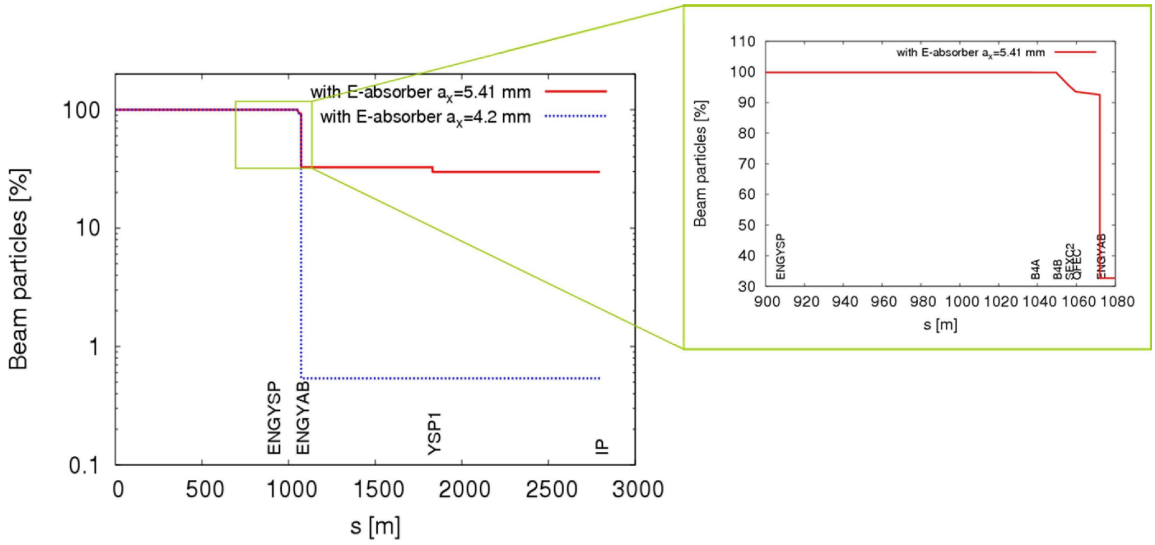

Figure 13. Left: number of beam particles along the CLIC BDS, considering an initial beam composed by 50000 macroparticles with 1.5% centroid energy offset and 1% full width of energy spread. Multiple Coulomb scattering within the E-spoiler (ENGYSP) increases the angular divergence. Perfect absorption of the beam is considered at the downstream E-absorber (ENGYAB) and at other limiting apertures of the lattice. Notice the logarithmic vertical scale. The cases for E-absorber apertures $a_x = 5.41$ mm and $a_x = 4.2$ mm are shown. Right: zoom of the particle losses in the section between ENGYSP and ENGYAB.

Macroparticles with high transverse amplitude have been tracked along the CLIC BDS using the code PLACET [17], taking into account the emission of synchrotron radiation and all the non-linear elements of the system. The particle positions and angles have been checked at the entrance, in the middle and at the exit of QF1 and QD0. Figure 15 shows the potentially dangerous particles (in red) according to the above conditions for different collimation apertures. The dangerous particles ("bad particles" in Fig. 15), i.e. particles which can generate unacceptable background at the IP, are efficiently removed for collimator aperture $< 15\ \sigma_x$ in the horizontal plane and $< 55\ \sigma_y$ in the vertical plane. Therefore, we have defined $15\ \sigma_x$ and $55\ \sigma_y$ as the transverse collimation depths.

Figure 16 shows the residual synchrotron radiation fans from the final quadrupoles QF1 and QD0 to the IP for an envelope covering 15 standard deviations in x and 55 in y. At the IP the photon cone is inside a cylinder with radius of 5 mm, which is within the beam pipe radius♯. Therefore, in principle, they are not an issue of concern from the detector point of view.

It should be considered whether swapping the betatron and energy collimation sections (see Fig. 17) may lead to further improvement on the betatron cleaning

♯ For the CLIC ILD (4 Tesla solenoid) detector configuration [24] the inner beam pipe radius at the IP is 29.4 mm, and for the CLIC SiD (5 Tesla solenoid) detector configuration [25] the radius is 24.5 mm [26].

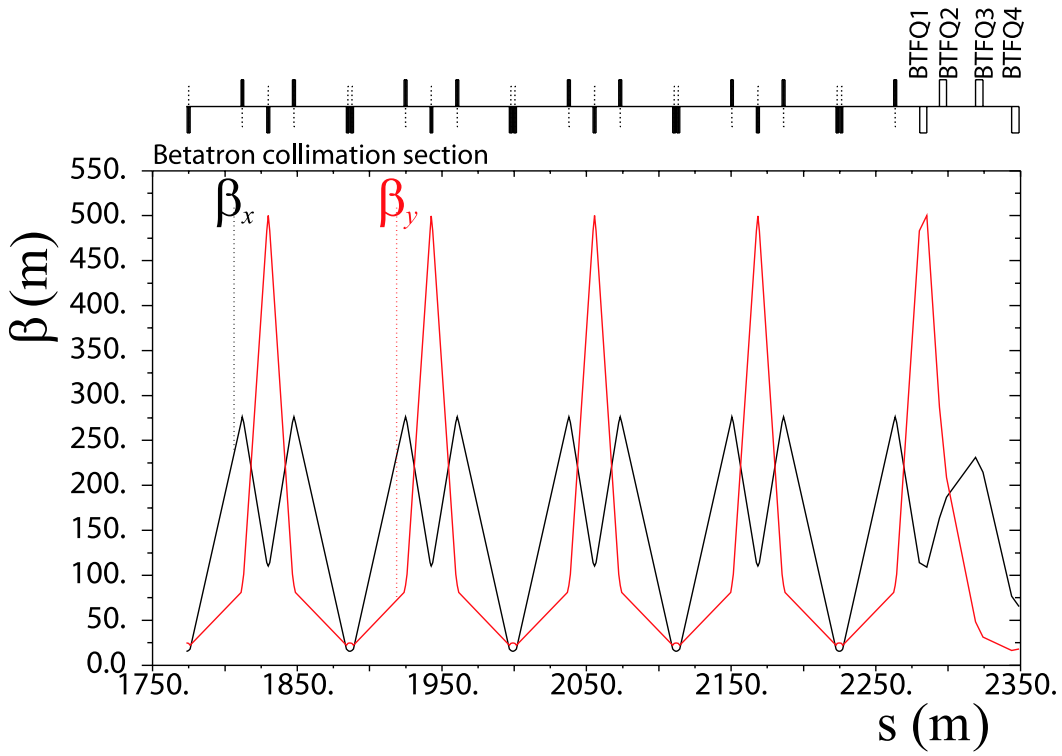

Figure 14. Optical functions of the CLIC betatron collimation section.

efficiency. This issue has recently been investigated by means of sophisticated tracking simulations, taking into account the halo generation by beam-gas scattering (Mott scattering) and inelastic scattering (Bremsstrahlung) in both linac and BDS, and the production of secondaries [9]. These simulations indicate that the effect of swapping the betatron and energy collimation sections results only in modest 40% reduction in the muon flux reaching the detector. We have decided to maintain the original order of location of the collimation sections in the CLIC BDS. In this way, errant beams coming from the linac would first hit the energy collimators before arriving to the betatron collimation part. In this sense, the energy collimators would protect the betatron collimators of possible damaging.

3.1. Spoiler design and absorber protection

The betatron spoilers must scrape the transverse beam halo at the required collimation depths. They must further provide enough beam angular divergence by MCS to decrease the transverse density of an incident beam, thus reducing the damage probability of the downstream absorber. By using similar arguments as in Section 2.1.1, for the protection of the CLIC betatron absorbers, which are made of Ti alloy coated by a thin Cu layer, the rms radial beam size $\sigma_r(s_{ab}) = \sqrt{\sigma_x(s_{ab})\sigma_y(s_{ab})}$ must be larger than about 600 μm at the absorber position [4, 16]. This condition determines the necessary minimum length of the betatron spoiler.

Table 7. Optics and beam parameters at collimator position: longitudinal position, horizontal and vertical β-functions, horizontal dispersion, horizontal and vertical rms beam sizes. YSP# denotes vertical spoiler, XSP# horizontal spoiler, YAB# vertical absorber and XAB# horizontal absorber.

Name	s [m]	β_x [m]	β_y [m]	D_x [m]	σ_x [μm]	σ_y [μm]
YSP1	1830.872	114.054	483.252	0.	5.064	1.814
XSP1	1846.694	270.003	101.347	0.	7.792	0.831
XAB1	1923.893	270.102	80.905	0.	7.793	0.742
YAB1	1941.715	114.054	483.185	0.	5.064	1.814
YSP2	1943.715	114.054	483.189	0.	5.064	1.814
XSP2	1959.536	270.002	101.361	0.	7.791	0.831
XAB2	2036.736	270.105	80.944	0.	7.793	0.743
YAB2	2054.558	114.054	483.255	0.	5.064	1.814
YSP3	2056.558	114.054	483.253	0.	5.064	1.814
XSP3	2072.379	270.003	101.347	0.	7.791	0.831
XAB3	2149.579	270.102	80.905	0.	7.793	0.742
YAB3	2167.401	114.054	483.185	0.	5.064	1.814
YSP4	2169.401	114.054	483.189	0.	5.064	1.814
XSP4	2185.222	270.002	101.361	0.	7.791	0.831
XAB4	2262.422	270.105	80.944	0.	7.793	0.743
YAB4	2280.243	114.055	483.255	0.	5.064	1.814

Considering the linear transport between a betatron spoiler and its corresponding downstream absorber, the expected value of the square of the transverse displacements at the absorber can be approximated by:

$$\langle x_{ab}^2 \rangle \simeq R_{12}^2(s_{sp} \rightarrow s_{ab})\phi_{MCS}^2 \ , \tag{16}$$

$$\langle y_{ab}^2 \rangle \simeq R_{34}^2(s_{sp} \rightarrow s_{ab})\phi_{MCS}^2 \ , \tag{17}$$

where ϕ_{MCS} is the angular divergence given by MCS in the spoiler. R_{12} and R_{34} are the transfer matrix elements between the betatron spoiler and the betatron absorber. In this case, $R_{12}(s_{sp} \rightarrow s_{ab}) = 114.04$ m and $R_{34}(s_{sp} \rightarrow s_{ab}) = -483.22$ m from YSP1 to YAB1 (see spoiler names in Table 7). Taking into account $\sigma_x(s_{ab}) = \sqrt{\langle x_{ab}^2 \rangle}$ and $\sigma_y(s_{ab}) = \sqrt{\langle y_{ab}^2 \rangle}$, and Eqs. (16) and (17), the condition for the survival of the betatron absorber can be written as follows:

$$\sqrt{|R_{12}(s_{sp} \rightarrow s_{ab})||R_{34}(s_{sp} \rightarrow s_{ab})|}\phi_{MCS} \gtrsim 600 \ \mu\text{m} \ , \tag{18}$$

which is fulfilled if $\phi_{MCS} \gtrsim 3 \times 10^{-6}$ rad. From this constraint and using Eq. (4) we can calculate the minimum length of spoiler material seen by an incident beam in order to guarantee the absorber survival. This condition is fulfilled if the Be spoiler is designed

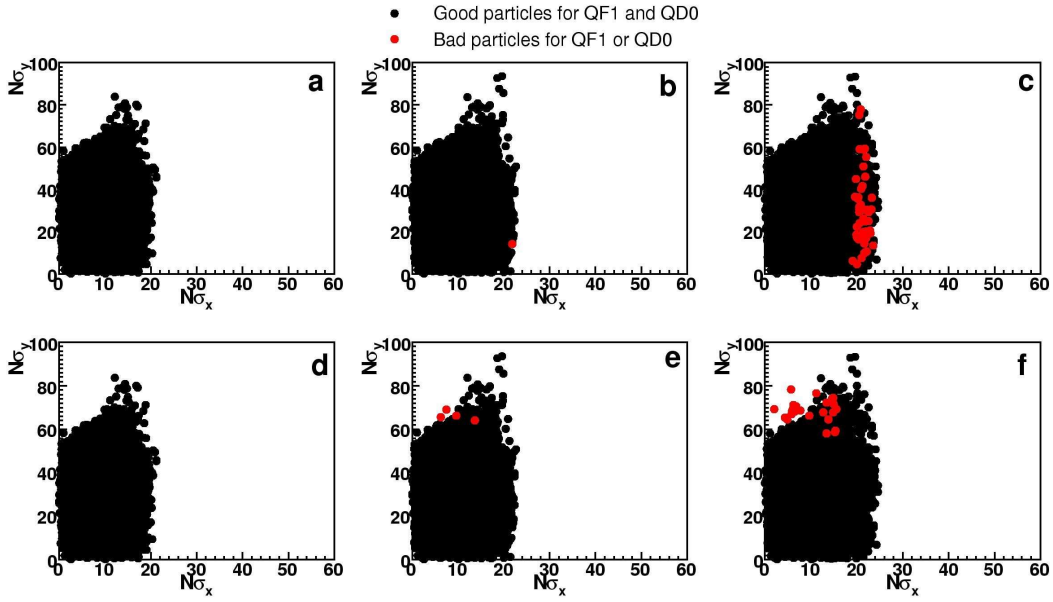

Figure 15. (Colour) Transverse beam distribution at the BDS entrance: non-dangerous macroparticles for the final doublet magnets are in black and potentially dangerous macroparticles are in red, according to different collimator apertures. The axes show the position of the particles in number of sigma in the x–x' and y–y' planes. In the following the corresponding horizontal and vertical collimator apertures (half gaps $a_{x,y}$) are given: a) $a_x = 0.11$ mm (13.7 σ_x) and $a_y = 0.08$ mm (44 σ_y), b) $a_x = 0.12$ mm (15 σ_x) and $a_y = 0.08$ mm, c) $a_x = 0.13$ mm (16.2 σ_x) and $a_y = 0.08$ mm, d) $a_x = 0.08$ mm (10 σ_x) and $a_y = 0.09$ mm (49.5 σ_y), e) $a_x = 0.08$ mm and $a_y = 0.10$ mm (50 σ_y), f) $a_x = 0.08$ mm and $a_y = 0.11$ mm (60.5 σ_y).

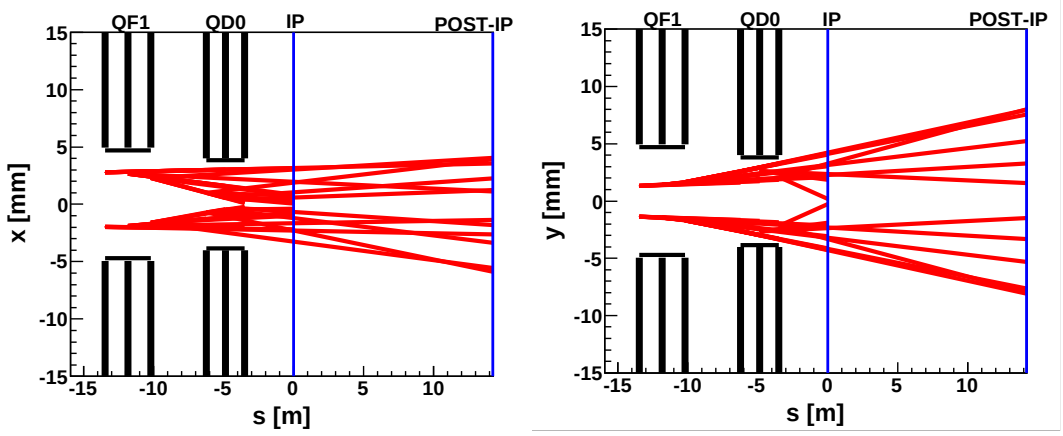

Figure 16. Synchrotron radiation fans in the CLIC interaction region emitted by particles with transverse amplitudes 15 σ_x and 55 σ_y (the betatron collimation envelope) in the final doublet magnets QF1 and QD0.

with a centre flat body of length $L_F \gtrsim 0.1\ X_0$. For instance, selecting a spoiler with $L_F = 0.2\ X_0$ could give a safe margin of angle divergence by MCS for absorber survival

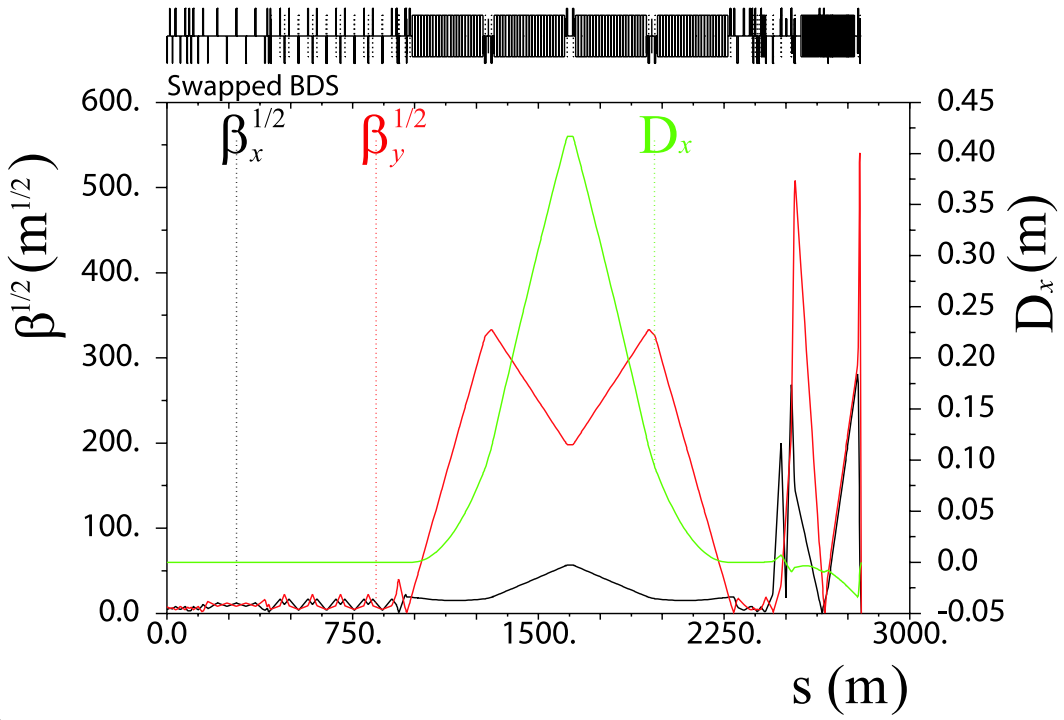

Figure 17. Optical functions of the CLIC beam delivery system with swapped lattice, i.e. the betatron collimation system upstream of the energy collimation section.

in case of beam impact.

Concerning the betatron spoiler protection for CLIC, it is worth mentioning that while the survival condition is important for the energy spoiler (see Sections 2.1.2 and 2.1.3), it is not restrictive for the betatron spoilers. These spoilers are planned to be sacrificial, i.e. they would certainly be destroyed if they suffer the direct impact of a bunch train. Direct impacts on the betatron spoilers are expected to be infrequent events. Large betatron oscillations of on-energy beams are not easily generated from pulse to pulse, and in the linac they rapidly filament and emittance can increase by 2 orders of magnitude.

In the hypothetical case that survivability of the betatron spoilers is desired, the betatron functions at the spoilers would have to be increased in order to enlarge the beam spot size sufficiently to ensure the spoiler survival. Nevertheless, this would increase the chromaticity of the lattice and generate tighter tolerances.

For CLIC the betatron spoilers have always been assumed to be made of Be. The main arguments to select Be were its high thermal and mechanical robustness and good electrical conductivity (to minimise resistive wakefields). Nevertheless, an important inconvenience of using Be is that its manipulation presents important technical challenges due to the toxicity of Be-containing dusts. An accident involving Be might be a serious hazard. Since no survivability to the full beam power is demanded for the betatron spoilers, the robustness condition of the material could be relaxed, and different options other than Be could be investigated, e.g. Ti with Cu coating.

If we decide to select a Ti based spoiler for betatron collimation, then, for absorber protection, the condition (18) is fulfilled if the spoiler is designed with a centre flat body (made of Ti) of length $L_F = 0.2\ X_0 \simeq 7$ mm.

Other proposals, such as rotating consumable collimators†† [29] and dielectric materials [30], are being investigated as alternative for future upgrades of the design.

Table 8 shows the design parameters of the CLIC betatron spoilers and absorbers (of the baseline system) after optimisation.

Table 8. Design parameters of the CLIC betatronic spoiler and absorbers.

Spoilers		
Parameter	XSP#	YSP#
Geometry	Rectangular	Rectangular
Hor. half-gap a_x [mm]	0.12	8.0
Vert. half-gap a_y [mm]	8.0	0.1
Tapered part radius b [mm]	8.0	8.0
Tapered part length L_T [mm]	90.0	90.0
Taper angle θ_T [mrad]	88.0	88.0
Flat part length L_F [radiation length]	0.2	0.2
Material (other options?)	Be (Ti–Cu coating?)	Be (Ti–Cu coating?)
Absorbers		
Parameter	XAB#	YAB#
Geometry	Circular	Circular
Hor. half-gap a_x [mm]	1.0	1.0
Vert. half-gap a_y [mm]	1.0	1.0
Tapered part radius b [mm]	8.0	8.0
Tapered part length L_T [mm]	27.0	27.0
Taper angle θ_T [mrad]	250.0	250.0
Flat part length L_F [radiation length]	18.0	18.0
Material	Ti alloy–Cu coating	Ti alloy–Cu coating

3.2. Optics optimisation

By design the phase advance of the betatron spoilers respect to the FD and the IP has to be matched to allow an efficient collimation of the transverse halo. The transverse phase advance between the spoiler positions and the IP is generally set to be $n\pi$ or $(1/2+n)\pi$, with n an integer. Figure 18 illustrates the design transverse phase advances of the CLIC betatron spoilers. The IP is at $\pi/2$ phase advance from the FD, and the phase

†† Rotatable collimators are currently being constructed for the collimation upgrade of the Large Hadron Collider (LHC) [28]. The LHC collimation experience will be useful to guide the technical design, construction and upgrade of the CLIC collimators.

relationship between the betatron collimators and the FD is crucial. The spoilers XSP1 (YSP1) and XSP3 (YSP3) are set to collimate amplitudes at the FD phase, while the spoilers XSP2 (YSP2) and XSP4 (YSP4) collimate amplitudes at the IP phase.

In the CLIC lattice version 2008 the phase advances between the fourth set of spoilers (YSP4 and XSP4) and the FD were not an exact multiple of $\pi/2$: $\Delta\mu_{x,y}^{SP4\to FD} = 9.7\pi/2, 10.6\pi/2$. Starting from this original lattice, and following a similar phase optimisation procedure as it was used for the ILC [31, 32], we have investigated phase-matched solutions between the fourth set of spoilers and the FD in order to further improve the collimation performance of the system. In this study the software MAD [33] has been used to model the lattice and perform the phase matching. In total eight quadrupoles have been used for the matching: four of them (BTFQ1, BTFQ2, BTFQ3 and BTFQ4) at the end of the betatron collimation section (Fig. 14) and four quadrupoles (QMD11, QMD12, QMD13 and QMD14) at the beginning of the FFS. Here the quadrupoles are named as in the CLIC lattice repository of Ref. [34]

The collimation performance of the lattices has been evaluated from beam halo tracking simulations using the code MERLIN [35]. For the tracking a "toy" model of the primary beam halo, consisting of 25000 macroparticles with energy 1500 GeV and zero energy spread, was generated at the BDS entrance, uniformly distributed in the phase spaces x–x' and y–y' and extending to 1.5 times the collimation depth. The halo has been tracked from the BDS entrance to the IP, treating the collimators as perfect absorbers of any incident particle. A measure of the primary collimation efficiency is the number of particles outside the collimation depth at the FD. A phase-matched solution has been found at $\Delta\mu_{x,y}^{SP4\to FD} = 10\pi/2, 11\pi/2$, which reduces the "escaped particles" (outside the collimation window) by 20% with respect to the original lattice. The strength values of the matching quadrupoles of the optimised lattice are shown in Table 9, compared with the initial values of the original lattice. The pole tip radius aperture for these quadrupoles is 8 mm. The effective lengths of the quadrupoles are 5 m for the BTFQ# type quadrupole and 1.63 m for QMD#. Figure 19 compares the halo x–y profile at the FD entrance for the original and the new matched lattices.

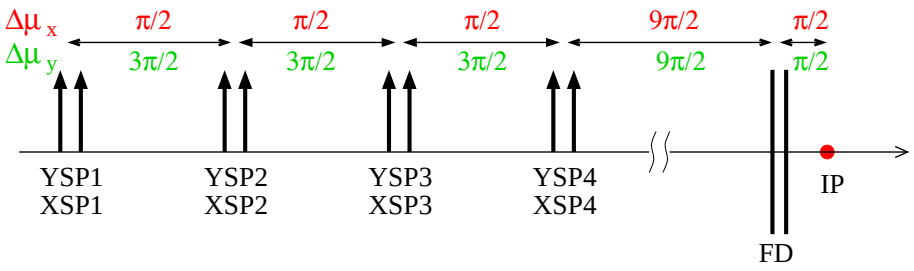

Figure 18. Schematic showing the design values of the phase advance between the betatron spoilers, FD and IP.

In addition to the collimation optimisation, it is necessary to evaluate the impact of the lattice changes on the luminosity. It is important that the lattices optimised

Table 9. Strength of matching quadrupoles in the transition region between the betatron collimation section and the final focus system for the original lattice and for the optimised lattice. K and B_0 denote the integrated quadrupole strength and the pole tip magnetic field, respectively.

	Original		Optimisation	
Name	K [m^{-1}]	B_0 [T]	K [m^{-1}]	B_0 [T]
BTFQ1	-0.0605	0.48432	-0.0669	0.5356
BTFQ2	0.0152	0.1217	0.0386	0.309
BTFQ3	0.0252	0.2017	0.0285	0.2281
BTFQ4	-0.0333	0.2666	-0.0731	0.5852
QMD11	0.0905	2.2224	0.1551	3.8087
QMD12	-0.1423	3.4944	-0.1023	2.5121
QMD13	0.1095	2.6889	0.0961	2.3599
QMD14	-0.0502	1.2327	-0.0736	1.8074

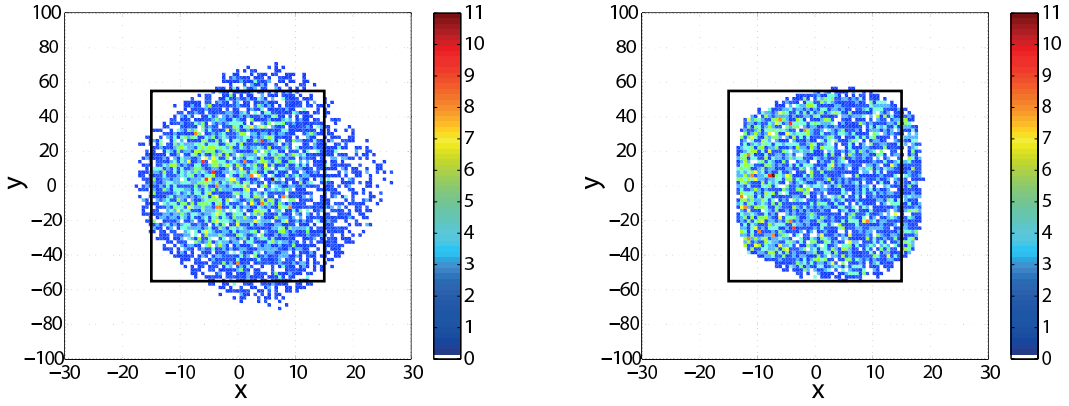

Figure 19. Beam halo x–y profile at the entrance of the FD (Left) and after (Right) optimisation. In this example no beam energy spread has been considered. The black square contour represents the collimation window.

for collimation maintain good properties for beam luminosity. We have calculated the luminosity peak from beam-beam interaction simulations at the IP by using the code GUINEA-PIG [36] for both the original and the optimised lattices. For the tracking of a Gaussian core beam with a uniform energy distribution of 1 % full energy spread, results show that the luminosity peak of the optimised lattice (for betatron collimation) is 1.5 times smaller than the luminosity of the original lattice. In principle, the luminosity performance can be recovered by adjusting slightly the strengths of the final focus sextupoles as it was made for the ILC BDS optimisation [32]. For these tracking simulations and luminosity calculations the CLIC BDS lattice of $L^* = 3.5$ m (available at the CLIC lattice repository [34]) has been used, where L^* is the distance from the final quadrupole QD0 to the IP.

4. Wakefield effects

A charged particle moving in an accelerator induces electromagnetic fields which interact with its environment. Depending on the discontinuities and variations in the cross-sectional shape of the vacuum chamber, the beam self field is perturbed and can be reflected onto the beam axis and interact with particles in the beam itself. These electromagnetic fields, induced by the charged beam, are called wakefields, due to the fact that they are left mainly behind the driving charge (the source charge of the wakefield). In the limit of ultra-relativistic motion the wakefields can only stay behind the driving charge.

In the case of bunched beams, depending on whether the wakefields interact with the driving bunch itself or with the following bunches, they are denominated *short range wakefields* or *long range wakefields*, respectively. The former may degrade the longitudinal and transverse emittances of individual bunches and the latter may cause collective instabilities.

Wakefields in the BDS of the linear colliders can be an important source of emittance growth and beam jitter amplification, consequently degrading the luminosity. The main contributions to wakefields in the BDS are:

- Geometric and resistive wall wakefields of the tapered and flat parts of the collimators.
- Resistive wall wakes of the beam pipe, which are especially important in the regions of the final quadrupoles, where the betatron functions are very large.
- Electromagnetic modes induced in crab cavities. Crab cavities are needed to rotate the train bunches in order to compensate for the crossing angle at the IP, which is 20 mrad in the case of CLIC.

In this report we focus on single bunch effects of the collimator transverse wakefields.

The main contribution to the collimator wakefields arises from the betatron spoilers, whose apertures (≈ 100 μm) are much smaller than the design aperture of the energy spoiler (3.5 mm), and much smaller than the aperture of the nearby vacuum chamber (8–10 mm radius).

In order to study the impact of the CLIC collimator wakefields on the beam, a module for the calculation of the collimator wakefields in different regimes has been implemented in the PLACET tracking code [37]. Using this code the effects of the collimator wakefields on the luminosity have been evaluated for the design transverse collimation apertures 15 σ_x and 55 σ_y. Figure 20 compares the relative luminosity degradation as a function of initial vertical position offsets at the entrance of the BDS with and without collimator wakefields. In this calculation the join effect of all the BDS collimators has been considered. For instance, for beam offsets of $\approx \pm 0.4$ σ_y, the CLIC luminosity loss was found to amount up to 20% with collimator wakefields, and up to 10% for the case with no wakefield effects.

The luminosity loss due to horizontal misalignments (with respect to the on-axis beam) of each horizontal spoiler and absorber is shown in Fig. 21 (Top). In comparison with the betatron collimators the energy spoiler (ENGYSP) and the energy absorber (ENGYAB) have been set with a large half gap, and practically do not contribute to the luminosity degradation by wakefields. On the other hand, for the horizontal betatron spoilers $\approx 20\%$ luminosity loss is obtained for $\approx \pm 50$ μm bunch-collimator offset.

In the same way, Fig. 21 (Bottom) shows the relative luminosity as a function of the vertical bunch-collimator offset for each vertical betatron spoiler. The stronger wake kick effects arise from the spoilers YSP1 and YSP3. Approximately 20% luminosity loss is obtained for vertical bunch-collimator offsets of $\approx \pm 8$ μm.

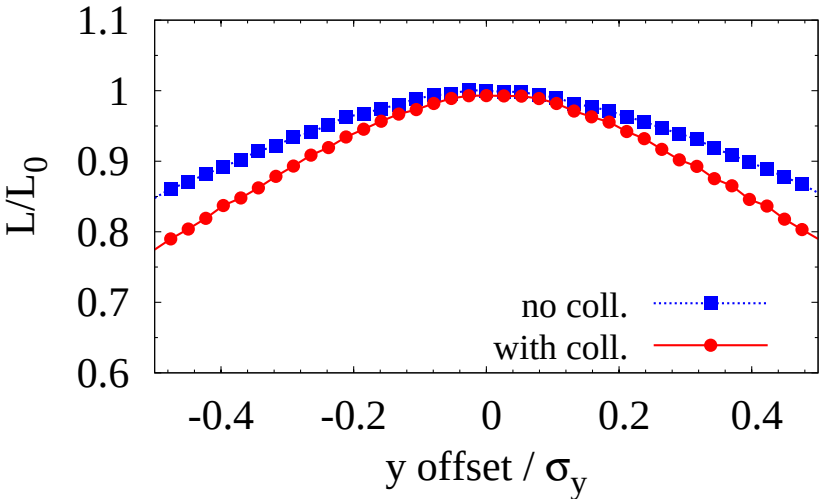

Figure 20. Relative CLIC luminosity versus initial beam offsets for the cases with and without collimator wakefield effects.

In order to optimise the spoiler design and thus reduce the wakefield effects, the following items could be investigated:

- Decreasing the geometrical wakes by optimising the spoiler taper angle.
- Coating the main body of the spoiler with a very thin layer of a very good electrical conductor.
- Exploring novel concepts, e.g. dielectric collimators [30].

4.1. Spoiler taper angle optimisation

Let us consider a beam with centroid offset y_0 from the beam axis passing through a symmetric spoiler of minimum half gap a. Assuming $y_0 \ll a$, the mean beam deflection due to spoiler wakefields can be expressed as follows:

$$\langle y' \rangle = \frac{r_e N_e}{\gamma} \kappa y_0 \ , \tag{19}$$

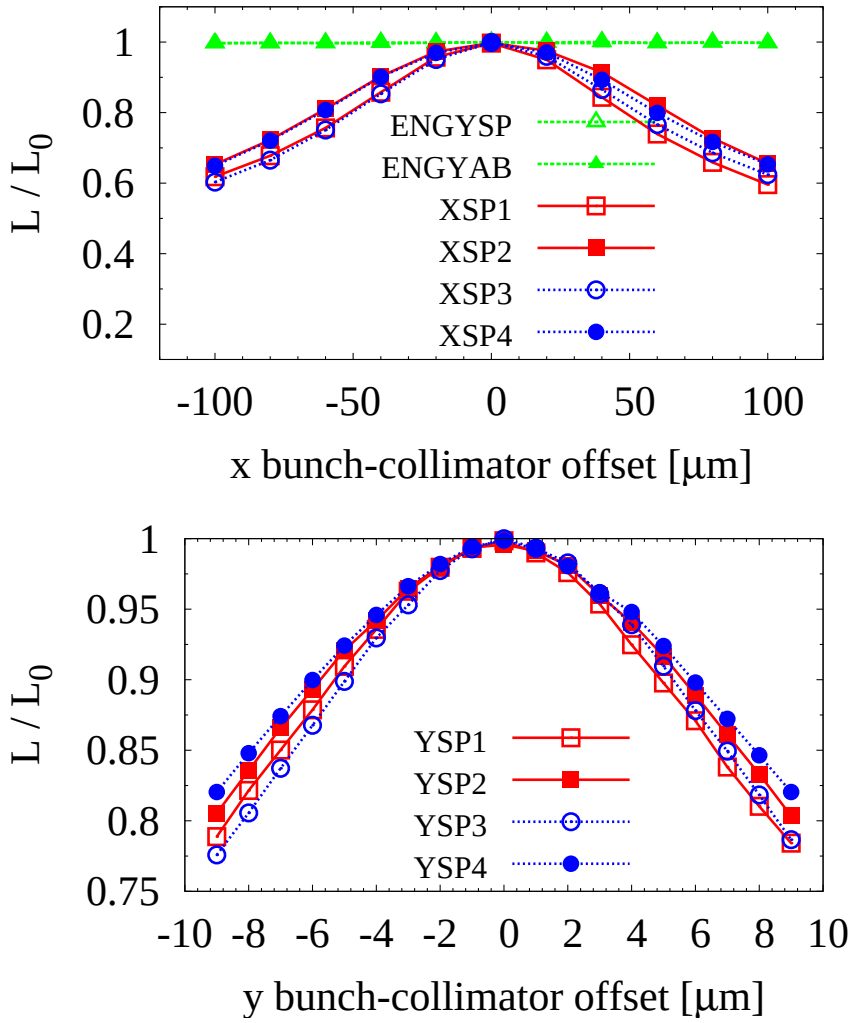

Figure 21. Top: relative luminosity versus horizontal bunch-collimator offset for each rectangular horizontal collimator. Bottom: relative luminosity versus vertical bunch-collimator offset for each rectangular vertical collimator.

where r_e is the electron classical radius, N_e the number of particles per bunch and $\gamma \equiv E/(m_e c^2)$ the relativistic Lorentz factor, with E the beam energy, m_e the rest mass of the electron and c the speed of light. In this equation the beam deflection has been given in terms of a transverse wake kick factor $\kappa = \kappa_g + \kappa_r$, which can be expressed as the sum of a geometrical wake kick contribution, κ_g, and another kick factor taking into account the resistive wall contribution, κ_r.

The spoilers are commonly designed with shallow taper angles in order to reduce the geometrical component of the wakefields. The taper angle is 88 mrad in the current design of the betatron spoiler (see Table 8). Here we investigate the possibility of reducing the wakefield effects by optimising the taper angle of the spoilers and, in consequence, to improve the luminosity performance.

For the taper angle optimisation we have to take into account the different collimator wakefield regimes as the taper angle changes. The geometrical wake kick can be calculated using the following "near-centre" approximation for rectangular collimators [38]:

$$\kappa_g = \begin{cases} \sqrt{\pi}\theta_T h/(2\sigma_z)\left(1/a^2 - 1/b^2\right) & \text{for} \quad \theta_T < 3.1^2 a\sigma_z/h^2 \ , \\ 8/3\sqrt{\theta_T/(\sigma_z a^3)} & \text{for} \quad 0.37^2\sigma_z/a > \theta_T > 3.1^2 a\sigma_z/h^2 \ , \\ 1/a^2 & \text{for} \quad \theta_T > 0.37^2\sigma_z/a \ . \end{cases} \tag{20}$$

As before, b and a denote the maximum and minimum half gap of the collimator, respectively. Here, h denotes the half width of the gap in the non-collimating direction. In Eq. (20) the limit $\theta_T < 3.1^2 a\sigma_z/h^2$ corresponds to the inductive regime; $0.37^2\sigma_z/a > \theta_T > 3.1^2 a\sigma_z/h^2$ corresponds to the intermediate regime; and $\theta_T > 0.37^2\sigma_z/a$ the diffractive regime. Considering the parameters for the vertical betatron spoiler of CLIC (Table 8), Eq. (20) can be written as follows:

$$\kappa_g = \begin{cases} \sqrt{\pi}\theta_T h/(2\sigma_z)\left(1/a^2 - 1/b^2\right) & \text{for} \quad \theta_T < 7\times 10^{-4} \text{ rad} \ , \\ 8/3\sqrt{\theta_T/(\sigma_z a^3)} & \text{for} \quad 0.06 \text{ rad} > \theta_T > 7\times 10^{-4} \text{ rad} \ , \\ 1/a^2 & \text{for} \quad \theta_T > 0.06 \text{ rad} \ . \end{cases} \tag{21}$$

For flat rectangular tapered spoilers the kick factor corresponding to the resistive component of the collimator wakefield can be approximate by the following expression for very small beam offsets [39]:

$$\kappa_r \simeq \frac{\pi}{8a^2}\Gamma(1/4)\sqrt{\frac{2}{\sigma_z\sigma Z_0}}\left[\frac{L_F}{a} + \frac{1}{\theta_T}\right] \ , \tag{22}$$

where $Z_0 = 376.7\ \Omega$ is the impedance of free space and $\Gamma(1/4) = 3.6256$.
The wake kick generated by a CLIC betatron spoiler in the vertical plane as a function of the taper angle is represented in Fig. 22, where the geometric and the resistive contribution are shown separately. With taper angle 88 mrad the geometric kick is in the diffractive regime. One could expect to reduce the geometric wakes by reducing the taper angle. However, on the other hand, for CLIC the resistive wake kick is dominant, and it increases as $1/\theta_T$ as the taper angle is decreased.

The total wake kick, adding both geometric and resistive contributions, is shown in Fig. 23. For taper angles < 0.01 rad the total wake kick strongly increases due to the resistive wake dominance. For angles > 0.1 rad the wake kick is not very sensitive to the change in the taper angle and remains practically constant. In Fig. 23 one can also note that there is a minimum wake kick factor in between 0.01 and 0.02 rad. For example, in order to improve the performance of the system in terms of wakefields, a new taper angle of ≈ 15 mrad could be selected. However, doing this, it is also necessary to increase the total longitudinal length of the spoiler, $2L_T + L_F$, from 25 cm (for the original taper angle 88 mrad) to ≈ 1 m for the new taper angle. Therefore, decreasing the taper angle one has to deal with a longer spoiler, and, given the tiny aperture of the betatron spoilers, tilt errors in the spoiler alignment could have much more negative effects on the beam stability than those affecting shorter spoiler.

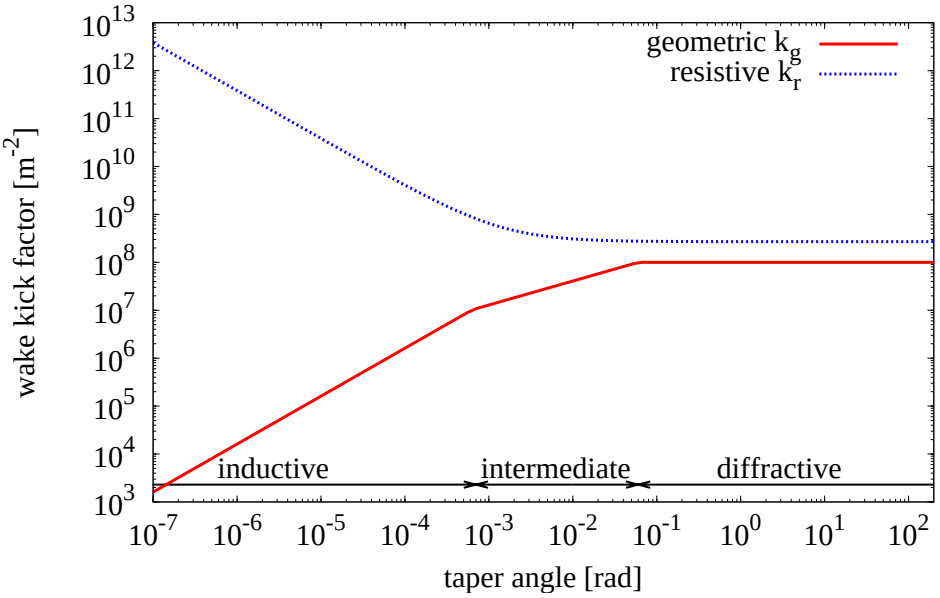

Figure 22. Geometric and resistive wake kick factors versus spoiler taper angle calculated from Eq. (21) and Eq. (22), respectively. The x–axis and y–axis are on logarithmic scale. The different regimes for the geometric wakefields are indicated.

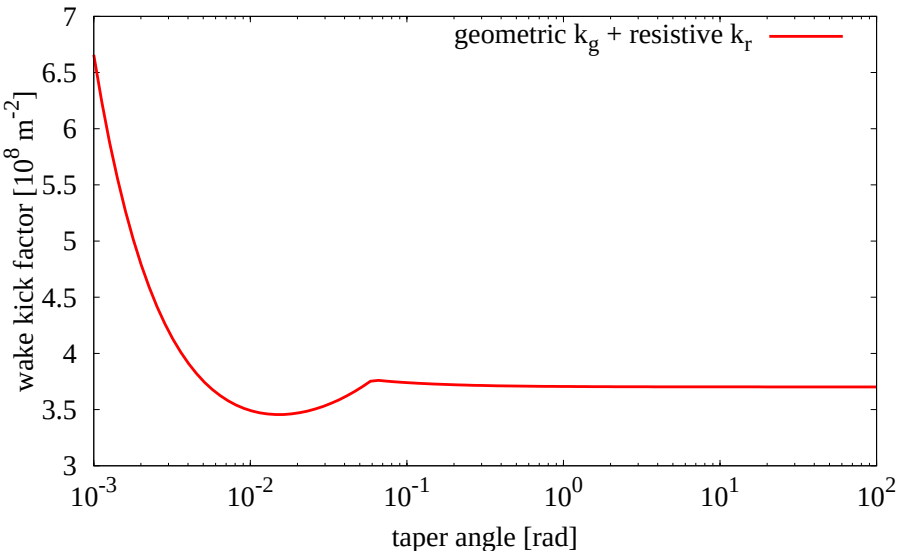

Figure 23. Total wake kick factor versus spoiler taper angle. The x–axis is on a logarithmic scale.

4.2. Betatron spoiler design review with regard to wakefields

In previous sections both energy and betatron spoilers have been considered made of Be. Beryllium was selected due to its high thermo-mechanical robustness as well as its high electrical conductivity in comparison with other metals. However, due to the highly toxicity of Be dust, special care must be taken when machining the material.

Since the betatronic spoilers are not required to survive the impact of an entire bunch train, i.e. they are planned to be sacrificial, in principle we could investigate optional materials other than Be for the betatronic spoiler design. Preliminary studies of spoiler design options with different geometry and combining different metals were shown in [40, 41]. For example, Ti alloy (90% Ti, 6% Al, 4% V) and Ti alloy with Cu coating could be good alternatives for the betatronic spoilers.

Be is better conductor than Ti: the electrical conductivity of Be at room temperature ($\sigma(\mathrm{Be}) \simeq 2.3 \times 10^7\ \Omega^{-1}\mathrm{m}^{-1}$) is one order of magnitude higher than the Ti conductivity ($\sigma(\mathrm{Ti}) \simeq 1.8 \times 10^6\ \Omega^{-1}\mathrm{m}^{-1}$). Therefore, in terms of wakefields Be is a better option than Ti. As we have seen in previous sections, for the current design of the CLIC spoilers, the main contribution to the wakefields is basically resistive. From Eq. (22) the dependence of the resistive wakefield kick on the electrical conductivity (σ) is given by $\kappa_r \propto 1/\sqrt{\sigma}$. The resistive wakefield kick by a Ti spoiler is almost four times bigger than the kick by a Be spoiler, $\kappa_r(Ti)/\kappa_r(Be) = \sqrt{\sigma(Be)}/\sqrt{\sigma(Ti)} \simeq 4$. On the other hand, the resistive kick produced by a Be spoiler is almost two times bigger than the kick by a spoiler made of Cu, $\kappa_r(Be)/\kappa_r(Cu) = \sqrt{\sigma(Cu)}/\sqrt{\sigma(Be)} \simeq 2$. Betatronic spoilers made of Ti coated with Cu could be a good option to reduce the impact of wakefields.

Other line of investigation, aimed to minimise the collimator wakefields, has recently started the design of dielectric collimators for the CLIC BDS [30]. Dielectric collimators are currently being designed for the second phase of collimation of the Large Hadron Collider (LHC) [42]. The plan is to adapt this concept also to the CLIC requirements. In [30] preliminary wakefield calculations have been made considering a cylindrical geometry model consisting of double layer based on a dielectric material coated with an external layer of copper.

4.3. Deflection due to surface roughness

As seen in Section 2.1.2, the impact of the full beam onto the Be spoiler might cause a permanent deformation of the spoiler surface. This could increase the wakefield effects and, therefore, to have negative consequences on the beam stability.

The average kick angle due to wakefield effects caused by the roughness of the spoiler/collimator surface can be estimated using the following expression for tapered surfaces [4]:

$$\langle x' \rangle_{\mathrm{rough}} \simeq \frac{4}{3a^2\pi^{3/2}} \frac{N_e r_e}{\gamma \sigma_z} \left[\frac{L_F}{a} + \frac{1}{\theta_T} \right] \zeta f \alpha_s x_0 \ , \tag{23}$$

where ζ is the characteristic size of the feature caused by the deformation, f is a form factor for the shape of the features, which is typically in the range between 1 and 20, α_s is the fraction of the surface filled with the features, N_e is the bunch population, r_e the electron classical radius, and x_0 the offset of the beam centroid with respect to the nominal beam axis. As in previous sections, a and b denote the minimum and maximum spoiler half gap, respectively. While in Ref. [4] only the tapered contribution ($1/\theta_T$) was

taken into account, here Eq. (23) takes into account the contributions from the tapered part and from the flat part (L_F/a).

According the ANSYS results of Section 2.1.2, horizontal deformation protuberances of about $\zeta \approx 1$ μm might be caused by tensile stress in the E-spoiler. We can roughly estimate the angular deflection using Eq. (23). For one hemispherical bump, the form factor $f = 3\pi/2$. For example, if we assume $\alpha_s \approx 1/3$ and $x_0 \approx 1$ σ_x (with $\sigma_x = 779$ μm at the E-spoiler), we obtain $\langle x' \rangle_{\rm rough} \simeq 4.8 \times 10^{-11}$ rad, which is approximately a factor 3 larger than the resistive wakefield kick $\langle x' \rangle_{\rm resistive} \simeq 1.8 \times 10^{-11}$ rad obtained from Eq. (22) for the same beam offset $x_0 \approx 1$ σ_x and for the E-spoiler.

If now we assume the same hypothetical level of deformation in a CLIC vertical betatronic spoiler made of Be, according Eq. (23), one obtains $\langle y' \rangle_{\rm rough} \simeq 3.6 \times 10^{-9}$ rad for a beam vertical deviation of 10 σ_y (with $\sigma_y = 1.814$ μm). This value is approximately 24% of the value obtained for the resistive wake kick, $\langle y' \rangle_{\rm resistive} \simeq 1.5 \times 10^{-8}$ for the same vertical beam offset.

5. Beam diagnostics in the collimation section

It is planned to set up beam position monitors (BPMs) at every quadrupole of the CLIC BDS and, therefore, each quadrupole of the collimation system will be equipped with one BPM of about 20–50 nm resolution. Sub-micron resolution levels can be achieved by using cavity BPMs. C-band and S-band type BPMs have been successfully commissioned and tested at the KEK final focus Accelerator Test Facility (ATF2) [43], achieving resolutions in the range 20-200 nm [44]. These BPMs will play a key role in the beam based alignment procedure of the collimation system and, in general, of the whole BDS. They will further form part of the necessary equipment for the implementation of orbit feedback systems for the BDS.

Beam loss monitors (BLMs) distributed along the collimation system would be useful to quantify the beam losses. These BLMs would be integrated into a global machine protection system, which would abort machine operation or activate the necessary protection mechanisms if intolerable levels of radiation are detected. The details of this system will be specified during the technical design phase.

Another important diagnostic instrument foreseen to be located into the collimation section is the post-linac energy spectrometer. The post-linac energy measurement has been devised in a way to minimise the required space due to the tight constraints in the CLIC total length. The deflection by the first dipole in the energy collimation section, together with three high precision BPMs, provides a compact spectrometer for energy measurement. A conceptual layout of this system is shown in Fig. 24. The energy measurement resolution of the set up is estimated to be $\approx 0.04\%$. The integrated magnetic field is assumed to have a calibration error of $\Delta(BL)/BL \approx 0.01\%$ and the BPM resolution is 100 nm. In addition, the energy collimation lattice incorporates a pulsed kicker magnet and a beam dump point, which can extract the beam dowstream of the energy diagnostic station. This permits the linac commissioning without requiring

the beam to pass through the IP.

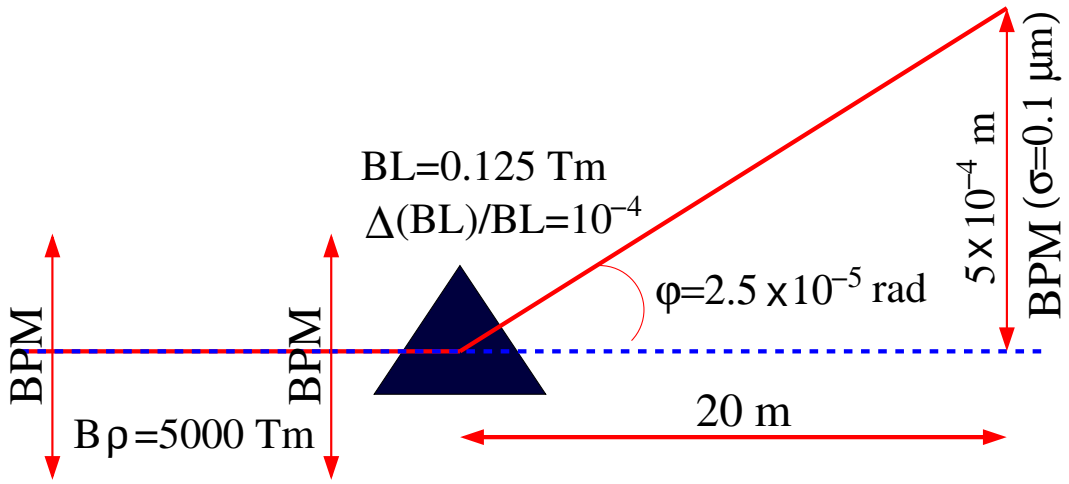

Figure 24. Conceptual compact CLIC energy measurement.

The CLIC energy collimation section has also a suitable drift space between the collimation dipoles to locate an upstream Compton based polarimeter [45]. It consists of a laser crossing point at position $s = 742$ m and a Compton electron detector at $s = 907$ m, behind 12 dipoles. This system would allow polarimetry from 1.5 TeV down to 135 GeV beam energies, but would require several wide-aperture dipoles. If we decide to locate the detector behind a lesser number of dipoles, the dipole aperture requirement would be reduced at the expense of reducing the reachable energy range, e.g. from 1.5 TeV down to 511 GeV, if the detector is placed behind 6 dipoles from the laser position. Ref. [45] concludes that for CLIC a standard Q-switched YAG laser operated with 100 mJ/pulse at 50 Hz would give adequate polarimeter performance.

6. Collimation system for CLIC at 500 GeV CM energy

The optics design of the CLIC BDS for 500 GeV CM energy can be found in the CLIC lattice repository of Ref. [34], where it is available in the format of the codes MAD [33] and PLACET [17]. For this energy option the collimation section is almost two times shorter than that of CLIC at 3 TeV. In total, the CLIC BDS length ratio for the options 0.5 TeV/3 TeV is 1.73 km/2.79 km.

No optimisation of the collimation parameters has yet been made for this option. In principle, the same collimation depths as well as the same number of collimators have been assumed for both 500 GeV and 3 TeV. The betatron functions, horizontal dispersion and rms beam sizes at each collimator position for the 500 GeV case are shown in Table 10.

For the CLIC optics at 500 GeV the dispersion D_x at the energy spoiler and absorber positions has been decreased $\approx 14\%$ with respect to the 3 TeV optics. Taking into account that the emittance dilution due to incoherent synchrotron radiation scale

Table 10. Optics and beam parameters at collimator position for CLIC at 500 GeV CM energy: longitudinal position, horizontal and vertical β-functions, horizontal dispersion, horizontal and vertical rms beam sizes. ENGYSP and ENGYAB denote the energy spoiler and the energy absorber, respectively. SP# denotes vertical spoiler, XSP# horizontal spoiler, YAB# vertical absorber and XAB# horizontal absorber. The rms horizontal beam size at the energy collimators has been calculated assuming a uniform energy distribution with 1% full energy spread.

Name	s [m]	β_x [m]	β_y [m]	D_x [m]	σ_x [μm]	σ_y [μm]
ENGYSP	453.549	703.166	35340.91	0.231	670.939	42.5
ENGYAB	536.049	1606.516	19635.742	0.357	1034.994	31.676
YSP1	915.436	57.027	241.653	0.	16.726	3.514
XSP1	923.347	135.001	50.678	0.	25.734	1.609
XAB1	961.946	135.051	40.446	0.	25.739	1.438
YAB1	970.857	57.027	241.565	0.	16.726	3.513
YSP2	971.857	57.027	241.567	0.	16.726	3.513
XSP2	979.768	135.001	50.676	0.	25.734	1.609
XAB2	1018.368	135.052	40.478	0.	25.739	1.438
YAB2	1027.279	57.027	241.655	0.	16.726	3.514
YSP3	1028.279	57.027	241.653	0.	16.726	3.514
XSP3	1036.19	135.001	50.679	0.	25.734	1.609
XAB3	1074.789	135.051	40.446	0.	25.739	1.438
YAB3	1083.7	57.027	241.565	0.	16.726	3.513
YSP4	1084.7	57.027	241.568	0.	16.726	3.513
XSP4	1092.611	135.001	50.676	0.	25.734	1.609
XAB4	1131.211	135.052	40.478	0.	25.739	1.438
YAB4	1140.122	57.027	241.655	0.	16.726	3.514

as $\Delta(\gamma\epsilon_x) \propto E^6 D_x^5/L^5$, where E is the beam energy and L the total length of the collimation lattice, then for the 500 GeV case the relative emittance growth ($\Delta\epsilon_x/\epsilon_x$) in the collimation system is expected to be about four orders of magnitude smaller than for the 3 TeV case. Table 11 compares the horizontal emittances growth and luminosity loss for the 500 GeV and 3 TeV cases as calculated using Eqs. (1) and (2).

Comparing the two energy cases, the following observations can be made:

- For CLIC at 500 GeV the beam power is 4.8 MW, which is $\approx$ 66% lower than that for CLIC at 3 TeV. Therefore, for CLIC at 500 GeV the damage potential of the beam (250 GeV beam energy) is smaller than that for the 3 TeV case (1.5 TeV energy beam), and more relaxed survival conditions can be considered for the energy spoiler. In this respect, materials with a lower fracture limit than Be may be chosen. A possible canditate might be Ti alloy.
- In order to minimise the multi-bunch effects of resistive wall in the CLIC BDS, the beam pipe radius was set at $b = 10$ mm for the 3 TeV case. Since for the

Table 11. Radiation integral I_5, relative emittance growth ($\Delta\epsilon_x/\epsilon_x$) and relative luminosity loss ($\Delta\mathcal{L}/\mathcal{L}$) due to synchrotron radiation in the collimation system and in the total BDS calculated for CLIC at 3 TeV and 0.5 TeV CM energy.

	CLIC 3 TeV		**CLIC 0.5 TeV**	
Variable	Coll. system	Total BDS	Coll. system	Total BDS
I_5 [m^{-1}]	1.9×10^{-19}	3.8×10^{-19}	5.6×10^{-18}	7.3×10^{-16}
$\Delta\epsilon_x/\epsilon_x$ [%]	13.5	27.3	0.0023	0.31
$\Delta\mathcal{L}/\mathcal{L}$ [%]	6.1	11.4	0.0012	0.15

CLIC at 500 GeV the beam charge is higher, the beam pipe radius has been set at $b = 12$ mm [23].

- Considering the same collimation depths 15 σ_x and 55 σ_y, Table 12 compares the collimator half gaps for both 500 GeV and 3 TeV options.
- The geometrical parameters of the collimators have to be calculated according the above minimum and maximum apertures. For instance, we can simply assume the same length for the collimators and then calculate the corresponding taper angles, $\theta_T = \tan^{-1}((b-a)/L_T)$.
- In this preliminary design the collimators (spoilers and absorbers) have been assumed to be made of similar materials and with the same geometrical structure as described in Sections 2 and 3.

Table 12. Half gaps of the CLIC post-linac collimators for the options at 3 TeV and 0.5 TeV CM energy. The values in parenthesis are new apertures suggested after optimisation.

	CLIC 3 TeV		**CLIC 0.5 TeV**	
Collimator	a_x [mm]	a_y [mm]	a_x [mm]	a_y [mm]
ENGYSP (E spoiler)	3.51 (2.5)	8.0	3.0	12.0
ENGYAB (E absorber)	5.41 (4.0)	8.0	4.6	12.0
YSP# (β_y spoiler)	8.0	0.1	12.0	0.19
YAB# (β_y absorber)	1.0	1.0	1.0	1.0
XSP# (β_x spoiler)	0.12	8.0	0.39	12.0
XAB# (β_x absorber)	1.0	1.0	1.0	1.0

Concerning collimator wakefields, for both CLIC at 3 TeV CM and CLIC at 0.5 TeV CM, considering the beam parameters of Table 1 and the collimator (spoiler) parameters of Table 8, the geometric wakefields (from Stupakov's criteria from Eq. (20)) are in the diffractive regime, near the border with the intermediate regime.

Taking into account the dependence of the resistive wake kick on the beam parameters and the collimator aperture (see Eq. (22)), $\langle y' \rangle \propto N_e/(E\sqrt{\sigma_z}a^3)$, the resistive

kick from the vertical betatron spoilers for 0.5 TeV CM is approximately a factor 1.25 larger than the kick for 3 TeV CM, $\langle y' \rangle_{0.5\ \mathrm{TeV}} / \langle y' \rangle_{3\ \mathrm{TeV}} \approx 1.25$. On the other hand, for the horizontal betatron spoilers the resistive kick ratio is $\langle x' \rangle_{0.5\ \mathrm{TeV}} / \langle x' \rangle_{3\ \mathrm{TeV}} \approx 0.25$.

No simulations have yet been carried out for the collimation performance study of the CLIC optics at 500 GeV CM. In this regard further work is needed.

7. Summary and outlook

The post-linac collimation system of CLIC must fulfil two main functions: the minimisation of the detector background at the IP by the removal of the beam halo, and the protection of the BDS and the interaction region against miss-steered or errant beams.

Recently several aspects of the CLIC post-linac collimation system at 3 TeV CM energy have been optimised in order to improve its performance. This report has been devoted to explain the optimisation procedure and to describe the current status of the CLIC collimation system.

The CLIC collimation system consists of two sections: one for momentum collimation and another one for betatron collimation. Next, the conclusions for the two sections are summarised.
For the energy or momentum collimation system:

- The energy collimation system of CLIC is designed to remove particles with off-energy $\gtrsim 1.3\%$ of the nominal beam energy. Furthermore, it is conceived as a system for passive protection against beams with large energy offsets ($\gtrsim 1.3\%$), caused by likely failure modes in the main linac.
- The design and optimisation of the energy collimators (spoiler and absorber) have been based on survival conditions. The energy collimators are required to survive the impact of an entire bunch train.
- A minimum spoiler length of 0.05 X_0 seems to provide enough transverse angular divergence by MCS to reduce the transverse beam density and guarantee the survivability of the downstream absorber in case of the impact of a bunch train.
- Beryllium has been selected to made the energy spoiler due to its high thermo-mechanical robustness as well as its high electrical conductivity (to reduce resistive wakefields) in comparison with other materials.
- Thermo-mechanical studies of the energy spoiler, based on the codes FLUKA [20] and ANSYS [21], have shown that fracture levels are reached if a bunch train hits the spoiler at $\sim 10\ \sigma_x$ horizontal offset from the beam axis. In the case of a more optimistic risk scenario, when a bunch train hits the spoiler at $\sim 5\ \sigma_x$, practically at the edge of the spoiler, the material does not fracture, but there might be permanent deformations. These deformations consist of horizontal protuberances of $\sim 1\ \mu$m. In principle, in terms of near-axis wakefields, a rough evaluation of the consequences of these deformations indicate negligible effects. However, for a more

precise evaluation, further studies of near-axis and near-wall wakefield effects are needed.

- From collimation efficiency studies, based on tracking simulations, the following conclusions can be drawn: increasing the beam pipe aperture from 8 mm to 10 mm seems to help to eliminate undesired residual beam losses in non-dedicated collimation places; reducing the energy collimator half gaps to 2.5 mm (spoiler) and 4 mm (absorber) has proved an optimal removal of beams with 1.5% mean energy offset and 1% full energy spread (for a uniform energy distribution).
- In the near-axis approximation, the wakefields generated by the energy collimators seem to have practically negligible effects on the luminosity.

For the betatron collimation system:

- The main function of the betatron collimation system is to provide the removal of those particles from the beam halo which can potentially contribute to generate experimental background at the IP.
- Beam tracking simulations have shown optimum betatronic collimation depths at 15 σ_x and 55 σ_y. For these depths the tracking simulations of a primary halo through the BDS have shown a good collimation efficiency of the system.
- An optimisation of the phase advance between the betatron spoilers and the final doublet has led to an additional 20% improvement of the cleaning efficiency.
- The betatron spoilers have to be set to relatively very narrow gaps (~ 100 μm) for efficient scraping of the transverse beam halo. Therefore, the surface of the jaws of these spoilers are very close to the beam axis, and can significantly contribute to the luminosity degradation by wakefields when the beam pass through them with a certain offset from the nominal beam axis. The luminosity loss due to collimator wakefields has been computed, using the codes PLACET [17] and GUINEA-PIG [36], and found to amount to up to 20% for vertical beam offsets of ≈ 0.4 σ_y. For this calculation spoilers made of Be have been assumed. This study has to be extended to other possible material options.
- Reducing the taper angle the geometrical contribution of the collimator wakefields is reduced. However, for the CLIC spoilers the resistive part of the wakefields is dominant, and only a very modest improvement in the minimisation of the wakefield effects has been found by reducing the taper angle to approximately 15 mrad. This translates into a longer spoiler (of almost 1 m) than the original 88 mrad spoiler (of 25 cm). Longer spoilers introduce tighter tolerances in terms of alignment and tilt errors. Therefore, we have finally decided to maintain the original taper angle of 88 mrad.
- For CLIC the betatron spoilers have always been assumed to be made of Be. The main arguments to select Be were its high thermal and mechanical robustness and good electrical conductivity (to minimise resistive wakefields). Nevertheless, an important inconvenience is the toxicity of Be-containing dusts, and accidents

involving Be might be a serious hazard. Since no survivability to the full beam power is demanded for the betatron spoilers (they are designed to be sacrificial or consumable), the robustness requirement of the material could be relaxed and different options other than Be could be taking into account. For example, Ti-Cu coating or Ti alloy-Cu coating could be good candidates.

For the collimation efficiency studies here we have assumed the spoilers as perfect collimators or 'black' collimators, considering the particles of the primary beam halo perfectly absorbed if they hit a spoiler or a limiting aperture in the BDS. In this simplification no secondary production have been assumed. However, in order to make more realistic simulations, the performance of the optimised CLIC collimation system has to be studied using specific simulation codes for beam tracking in collimation lattices, such as BDSIM [46]. The tracking code BDSIM allows us to make a more realistic collimation scenario adding the production of secondary particles and its propagation along the lattice when a particle of the primary halo hit one spoiler or other component of the lattice. Recently an interface BDSIM-PLACET [47] has also been developed for the tracking of the beam halo through the BDS of linear colliders, including the wakefield effects and the production of secondaries. In addition, simulations using a more realistic model of the transverse halo would also be convenient. In this direction, notable progress has been made during the last years on the investigation and simulation of different mechanisms which generate transverse halo in both linac and BDS of the linear colliders. The code PLACET incorporates a module called HTGEN [48], which permits the simulation of the production of beam halo by beam-gas scattering and the tracking of this halo and the beam core along the lattice. For a more complete characterisation, we plan to apply all these simulation tools to the optimised collimation system.

Measurements of collimator wakefields will be useful to validate the analytical and simulation results. In the past, sets of measurements have been made for longitudinally tapered collimators at SLAC End Station A (ESA), see for example [49]. For the geometric wakefields, these measurements showed an agreement at the level of 20% with the simulation results and good qualitative agreement with the theory, although in many cases there was a quantitative discrepancy as large as a factor 2 between theory and measurement. Measurements of the resistive wakefields [50] showed notable discrepances with theory. New sets of measurements would be helpful, using available beam test facilities, such as ATF2 [43], ESTB (former ESA) [51], CALIFES [52] and FACET [53]. For instance, a possibility would be the use of the test facility FACET at SLAC, which will operate with longitudinally short bunches (20 μm bunch length) and bunch charge (1 nC) close to those of CLIC (44 μm bunch length and 0.6 nC bunch charge).

For the CLIC option at 500 GeV CM energy the collimation system design is still in a premature state. In this sense, further work has to be made for its optimisation and consolidation.

Acknowledgements

This work is supported by the European Commission under the FP7 Research Infrastructures project EuCARD, grant agreement no. 227579.

References

[1] R. Tomás, "Overview of the Compact Linear Collider", Phys. Rev. ST-AB **13**, 014801 (2010).
[2] F. Tecker *et al.*, "CLIC 2008 parameters", CLIC-NOTE-764 (2008).
[3] D. Schulte and F. Zimmermann, "Failure Modes in CLIC", Proceedings of PAC 2001, Chicago; CLIC-NOTE-492 (2001), CERN-SL-2001-034 (AP) (2001).
[4] NLC Design Group, "Zeroth-Order Design Report for the Next Linear Collider," 573-574 (1996).
[5] R. Assmann *et al.*, "Overview of the CLIC Collimation Design", Proceedings of PAC 2001, Chicago, USA.
[6] R. Assmann *et al.*, "Collimation for CLIC", AIP Conf. Proc. Vo. 693, pp. 205-208, December 16, 2003.
[7] ILC Collaboration, "International Linear Collider Reference Desing Report. Volume 3: Accelerator", ILC-REPORT-2007-001, August, 2007.
[8] I. Agapov *et al.*, "Tracking studies of the Compact Linear Collider Collimation system", Phys. Rev. ST-AB **12**, 081001 (2009).
[9] L. Deacon *et al.*, "Muon backgrounds in CLIC", Proceedings of IPAC 2010, Kyoto, Japan, 2010.
[10] M. Jonker *et al.*, "The CLIC machine protection", Proceedings of IPAC 2010, WEPEB71, Kyoto, Japan, 2010.
[11] S. Fartoukh, J. B. Jeanneret and J. Pancin, "Heat deposition by transient beam passage in spoilers", CERN-SL-2001-012 AP, CLIC Note 477, 2001.
[12] M. Sands, "Emittance Growth from Radiation Fluctuations", SLAC/AP-47, December 1985.
[13] R. H. Helm, M. J. Lee and P. L. Morton, "Evaluation of Synchrotron Radiation Integrals", SLAC-PUB-1193, March 1973.
[14] B. Dalena *et al.*, "Solenoid and Synchrotron Radiation effects in CLIC", Proceedings of PAC 2009, Vancouver, Canada, 2009; EuCARD-CON-2009-059.
[15] Particle Data Group, Physics Letters B **667** (2008), p. 271.
[16] P. Tenembaum, "Studies of beam optics and scattering in the next linear collider post-linac collimation system", Proceedings of LINAC 2000, MOA08, (2000).
[17] https://savannah.cern.ch/projects/placet.
[18] S. M. Seltzer and M. J. Berger, "Improved Procedure for Calculating the Collision Stopping Power of Elements and Compounds for Electrons and Positrons", Int. J. Appl. Radiat. Isot. Vol **35**, No. 7, pp. 665-676 (1984).
[19] http://www.matweb.com. This website, widely used by the material engineering community, provides a very reputable source of material properties.
[20] A. Fasso *et al.*, "FLUKA: a multi-particle transport code", CERN-2005-10 (2005), INFN/TC-05/11, SLAC-R-773.
[21] http://www.ansys.com/ (ANSYS® v. 11.0 Academic Research)
[22] R. von Mises, "Mechanik der Festen Korper in plastisch deformablen Zustand," Göttin. Nachr. Math. Phys. vol. 1, pp. 582-592 (1913). (In German).
[23] R. Mutzner *et al.*, "Multi-bunch effect of resistive wall in the CLIC BDS", Proceedings of IPAC 2010, Kyoto, Japan, 2010.
[24] ILD Concept Group, "Letter of Intent for the International Large Detector": http://www.ilcild.org/documents/ild-letter-of-intent.
[25] H. Aihara *et al.*, "SiD Letter of Intent", arXiv:0911.0006 [physics.ins-det].
[26] André Sailer, private communication.

[27] N. Phinney, "SLC final performance and lessons", Proceedings of LINAC 2000, Ed. A. W. Chao, eConf C00082 (2000), MO102; arXiv:physics/0010008.
[28] J. C. Smith *et al.*, "Construction and Bench Testing of a Rotatable Collimator for the LHC Collimation Upgrade", Proceedings of IPAC 2010, Kyoto, Japan, 2010.
[29] J. Frisch, E. Doyle and K. Skarpaas, "Advanced Collimator Prototype Results for the NLC", SLAC-PUB-8463 (2000).
[30] A. Kanareykin *et al.*, "Dielectric Collimators for Linear Collider Beam Delivery System", Proceedings of IPAC 2010, Kyoto, Japan, 2010.
[31] F. Jackson, "Collimation Optimisation in the Beam Delivery System of the International Linear Collider", Proceedings of EPAC 2006, Edinburgh, Scotland, UK, 2006.
[32] F. Jackson at al., "Collimation Optimisation in the Beam Delivery System of the International Linear Collider", Proceedings of PAC 2007, Albuquerque, New Mexico, USA, 2007; EUROTeV-Report-2007-045 (2007).
[33] H. Grote and F. C. Iselin, "The MAD Program, User's Reference Manual", CERN/SL/90-13 (AP) (1996); see the web site: http://mad.home.cern.ch.mad.
[34] http://clicr.web.cern.ch/CLICr/MainBeams/BDS/.
[35] MERLIN homepage: http://www.desy.de/merlin/.
[36] D. Schulte, "study of electromagnetic and hadronic background in the interaction region of the TESLA collider", Ph.D. Thesis, University of Hamburg, Hamburg, Germany (1996), TESLA-97-08.
[37] G. Rumolo, A. Latina and D. Schulte, Proceedings of EPAC 2006, Edinburgh, Scotland, UK, 2006; EUROTeV-Report-2006-026 (2006).
[38] G. V. Stupakov, "High-frequency impedance of small-angle collimators", Proceedings of PAC 2001, Chicago.
[39] A. Piwinski, "Wake fields and ohmic losses in flat vacuum chambers", DESY-HERA-92-04 (1992).
[40] J. Resta-López and J. L. Fernández-Hernando, "Review of the CLIC Energy Collimation System and Spoiler Heating", EUROTeV-Report-2008-050 (2008).
[41] J. L. Fernández-Hernando and J. Resta-López, "Design of Momentum Spoilers for the Compact Linear Collider", Proceedings of PAC 2009, Vancouver, Canada, 2009.
[42] E. Metral *et al.*, "Impedance Studies for the Phase 2 LHC Collimators", Proceedings of PAC 2009, Vancouver, Canada, 2009.
[43] P. Bambade *et al.*, "Present status and first results of the final focus beam line at the KEK Accelerator Test Facility", Phys. Rev. ST-AB **13**, 042801 (2010).
[44] S. Boogert *et al.*, "Cavity Beam Position Monitor System for ATF2", Proceedings of IPAC 2010, Kyoto, Japan, 2010.
[45] K. P. Schüler, "Upstream polarimeter for CLIC", talk presented at the CLIC 2008 Workshop, CERN, Geneva, 14-17 October 2008.
[46] I. Agapov, G. A. Blair, S. Malton and L. Deacon, "BDSIM: A particle tracking code for accelerator beam-line simulations including particle-matter interactions", Nucl. Instrum. Methods Phys. Res. A, **606**, 708 (2009).
[47] G. Blair *et al.*, "Simulation of beam halo in CLIC collimation system", Proceedings EPAC 2008, Magazzini del Cotone, Genoa, Italy (2008).
[48] H. Burkhardt *et al.*, "Halo and Tail Generation Computer Model and Studies for Linear Colliders", EUROTeV-Report-2008-076;
Halo and tail generator packge HTGEN: http://hbu.home.cern.ch/hbu/HTGEN.html.
[49] P. Tenenbaum *et al.*, "Direct measurement of the transverse wakefields of tapered collimators", Phys. Rev. ST-AB **10** (2007), 034401.
[50] P. Tenenbaum and D. Onoprienko, "Direct Measurement of the Resistive Wakefield in Tapered Collimators", Proceedings of EPAC 2004, Lucerne, Switzerland, 2004.
[51] R. Erickson *et al.*, "ESTB End Station Test Beam. A Proposal to Provide Test Beams in SLAC's End Station A", July 31, 2009;

http://www-conf.slac.stanford.edu/estb2011/ESTB_Proposal%080309.pdf.

[52] W. Farabolini *et al.*, "CTF3 Probe Beam Linac Commissioning and Operations", Proceedings of LINAC 2010, Tsukuba, Japan, 2010.

[53] J. Amann *et al.*, "FACET, Conceptual Design Report", SLAC-R-930, September 14, 2009.